Supplementary Online Material for

Signaling network trigger and plasma membrane physical properties control actin cytoskeleton driven isotropic phase of cell spreading.

Padmini Rangamani[1], Marc-Antoine Fardin[2], Yuguang Xiong[1], Azi Lipshtat[1], Olivier Rossier[2], Michael P. Sheetz[2] and Ravi Iyengar[1]

[1]Department of Pharmacology and Systems Therapeutics, Mount Sinai School of Medicine, New York, NY 10029

[2]Department of Biological Sciences, Columbia University, New York NY 10027

Address all correspondence to:

Ravi Iyengar

Department of Pharmacology and Systems Therapeutics, Box 1215

Mount Sinai School of Medicine

One Gustave Levy Place

New York NY 10029

Phone: 212-659-1707

Fax: 212-831-0114

E-mail: ravi.iyengar@mssm.edu

Running title: Plasma membrane feedback controls signaling regulation of cell spreading

1. Construction of the signaling network

In order to construct the integrin-signaling network, we identified the proteins and components that are part of the signaling pathways and their immediate upstream and downstream components. This was done by an extensive literature search. The signaling network was limited to those components whose activities directly affect the dynamics of Arp2/3, gelsolin and G-ATP-actin. This simplification allows us to maintain the interface between signaling network and the motility machinery at a manageable level. The network was constructed in a modular fashion, allowing for the identification of the regulatory loops that can drive the dynamics.

The interaction network for integrin mediated signaling was constructed from primary literature and the Science Signaling map for the integrin signaling network (1). Overall, our interaction network consists of 84 biochemical reactions between 43 components. The complete list of reactions along with the references is provided in Table S1. The network was constructed in modules based on functional consequences of signaling. The focus of the signaling network is only on the dynamics of the actin remodeling proteins Arp2/3, profilin and gelsolin. The complete signaling network (Figures S1 and S2) was further divided into modules that follow the behavior of key components of interest. Modular construction of the network allowed us to constrain the network by comparing experimental and simulation results for timescales of activation and inactivation. This approach allows for assembly of larger networks from experimentally constrained models (Bhalla and Iyengar 1999). The biology of the individual modules is described briefly in the following sections.

1.1 Integrin-FAK-Src module

In this module, the immediate early events following integrin activation by fibronectin are included. When fibronectin or a similar extracellular matrix ligand binds to the integrin receptor, the receptors form clusters and are activated. We did not separately detail the different isoforms of integrin subunits or cluster formation and

mechanotransduction by the integrin receptors. This interaction is represented as a single reaction of integrin binding fibronectin. The activated receptor then binds FAK and leads to the activation of this kinase by autophosphorylation. FAK and Shp2 activate Src via phosphorylation and dephosphorylation respectively. FAK also activates Csk, the c-terminal Src kinase, which in turn inactivates Src. Therefore, FAK participates in both activation and inactivation of Src.

1.2 Talin-PIPKI module

In this module, the activation of Talin and PIP kinase type I leading to $PI(4,5)P_2$ synthesis are modeled. This is one of the early events associated with focal adhesion formation and the role of PIP kinase I in integrin signaling has been well-studied (2,3). Talin is activated by $PI(4,5)P_2$ and ligand-bound integrin receptor via a binding reaction. This activated talin is now capable of activating PIP kinase type I. Activation of PIP kinase leads to the synthesis of $PI(4,5)P_2$ forming a positive feedback loop. Shp-1 a phosphatase, inactivates PIPKI, and $PI(4,5)P_2$ inactivates Shp1.

1.3 Rho module

Rho is a small GTPase known to play an important role in stress fiber formation. Rho is activated by p190RhoGEF and inactivated by p190RhoGAP. Src indirectly down regulates Rho by phosphorylating and activating p190RhoGAP. Shp2 and PTP dephosphorylate p190RhoGAP. FAK activates p190RhoGEF by phosphorylating it. Combining these interactions with the Integrin-FAK-Src module allows for the study the complex role of Src and FAK in activation of Rho. RhoGTP activates PIPKI by binding and presenting it to Src for phosphorylation. Thus, the RhoGTP module also interacts with the Talin-PIPKI module. It should be noted that there are multiple GAPs and GEFs that can play a role in the GDP/GTP cycle and can act of many of the Rho-family GTPases. However, in this model, it is assumed that the GEFs and GAPs function exclusively for each small Rho-GTPase family member. A uniform spatial distribution of the Rho-GTPases is assumed.

1.4 Rac module

Rac plays an important role in the formation of lamellipodia. In this model, there are two Rac GEFs that are modulated by the upstream signaling processes. Tiam1 is activated by $PI(3,4,5)P_3$ and Dock/Elmo is activated by the force sensing scaffold protein p130Cas via Crk and also by RhoGTP providing the connection between the Rho and Rac modules. Src activates p130Cas and RacGAP via phosphorylation, thus playing a dual role in the activation and inhibition kinetics of Rac. Another loop exists between Rac and $PI(3,4,5)P_3$, where $PI(3,4,5)P_3$ activates Tiam1 and Rac activates PI3K, which is responsible for $PI(3,4,5)P_3$ synthesis.

1.5 Cdc42 module

Cdc42 is responsible for filopodia formation and activates N-WASP by directly binding to it. Src activates PIX/Cool, a Cdc42GEF (4). It is known that Cdc42GAP is activated by phosphorylation but not much is known about protein kinase involved. Therefore, we assumed that FAK phosphorylates and activates Cdc42GAP. The interaction of Src and FAK leads to complex dynamics as FAK directly activates Cdc42GAP and indirectly activates Cdc42GEF via Src.

1.6 Arp2/3 Module

Arp2/3 is a seven subunit complex that is responsible for binding to the side of an existing filament and nucleating a new filament branch. Arp2/3 is activated separately by N-WASP and WAVE. The branching mechanism, interaction with actin and orientation angle of the newly formed branch are well-documented (5-7). WASP activation requires binding of Cdc42 and $PI(4,5)P_2$, to relieve the inhibitory conformation of WASP (8). WAVE on the other hand does not have an inhibitory conformation but is activated by the binding of $PI(3,4,5)P_3$ and Rac (9).

1.7 Profilin Module

Profilin functions as a nucleotide exchange factor, promoting ATP exchange on G-ADP-actin. It is required for filament nucleation events; polymerization of actin filaments takes place only after a nucleus of 3 or more G-ATP-actin monomers is formed (10). Activation of profilin is carried out through a series of scaffolding proteins. The signal for profilin activation comes directly from activated integrin via a series of binding reactions. Integrin activates α-actinin, an actin bundling protein. Direct interactions with of α-actinin, zyxin and VASP with actin filaments or monomers are not considered in this model. Activated α-actinin binds to zyxin, which subsequently activates VASP. Activated VASP binds to profilin and activates it. $PI(4,5)P_2$ inhibits both profilin and α-actinin by direct binding interactions.

1.8 Gelsolin module

Gelsolin functions as a capping protein, capping the barbed ends of growing filaments. Gelsolin is inhibited by $PI(4,5)P_2$ binding. Gelsolin bound to $PI(4,5)P_2$ cannot cap existing actin filaments but free gelsolin can (11). Regulation of gelsolin depends on $PI(4,5)P_2$ and calcium kinetics regulated by upstream signaling. Gelsolin is activated by calcium release from the endoplasmic reticulum (12). Because the half-life of a capped filament is about 30 minutes (13), the deactivation of gelsolin during the isotropic spreading phase of about 5-8 minutes need not be considered.

2. Development of a multi-compartmental ordinary differential equation model for the signaling network

The interactions from the signaling network are converted to biochemical reactions (Table S1). The biochemical reaction network was translated into a multi-compartmental ordinary differential equation model in the Virtual Cell suite (14). Because the signaling network involves reactions in both the cytoplasm and the plasma plasma membrane, incorporating a measure of spatial dimension is important.

Compartmental models are used to limit components to specific compartments and interactions between components are resolved using flux definitions. The model cell has two main compartments - the plasma membrane and the cytoplasm. For purposes of calcium release, the endoplasmic reticulum is modeled as a distributed compartment in the cytoplasm. The full table of reactions and kinetic parameters along with assumptions and references is presented in Table S1. Table S4 lists the components that flux between different compartments as a result of reactions.

2.1 Kinetic parameters and initial concentrations

Many of the kinetic parameters including binding constants and enzymatic rate constants were obtained from the literature (Table S1). In some cases, the kinetic parameters were not available. For these reactions, the kinetic parameters were assumed to be in the same range as parameters for similar components. Sensitivity analysis for these assumed parameters showed that the dynamics of the signaling network was robust over a range of values tested.

For many components, we were also able to obtain estimates of the initial concentrations of the components (Table S2). In the cases where a literature reference for the initial concentration could not be found, estimates based on similar components were used.

2.2 Experimental Constraints of network dynamics

The dynamics of key components in the signaling network were validated against experimental data in the literature to ensure that the time courses from the simulations were in reasonable agreement with the experimental observations. The goal here was not to obtain an exact quantitative match but to determine if there was a qualitative agreement in the temporal dynamics of the activation/ deactivation profiles.

In order to validate the signaling dynamics, experimental data in published literature was used and the time course from the experiments was converted to

normalized activation kinetics using ImageJ software. The comparison was restricted to normalized concentrations because the exact concentration of the individual components was not known. In each case, the concentration dynamics from the literature was saved as as an image file that was loaded into ImageJ. Using the measurement tools in ImageJ, the concentrations of the active components were obtained at different time points. These values were then normalized using the maximum concentration to obtain dimensionless fraction of maximum concentrations. Similarly, the dynamics from the simulations were used within the same time range and normalized. The entire process is detailed in Figure S3.

As shown in Figure S4, the concentration profiles of the six components shown have a good agreement with the experimental observations. Although, the goal was to obtain the dynamics of Arp2/3, gelsolin and G-ATP-actin from the signaling model, the activation kinetics of Arp2/3 and gelsolin were not compared from the literature because the predominant experimental approach to measuring the experimental activity of Arp2/3 and gelsolin is the fluorescence measurement of actin polymerization (15,16). This is not the same as time course of Arp2/3 or gelsolin activation by their respective upstream signaling counterparts. The temporal profiles of FAK (17), Src (17), p130Cas phosphorylation (18), Cdc42 activation (19), Rac activation (19) and PLC-γ phosphorylation (20) from experiments were compared to the dynamic profiles from the ODE simulations. The experiments chosen for validation were based on integrin signaling, mostly in fibroblasts for cell spreading assays.

2.3: Variation of initial conditions

As noted in Table S2, some initial concentrations were assumed in the signaling model. The values were chosen to be within a physiologic range, based on values used in other models of signaling networks (Table S2). The values of these initial conditions were varied to test for the effect of the effect of varying initial conditions on the concentrations of Arp2/3, gelsolin and G-ATP-actin and the net rate of polymerization.

3. Development of a hybrid model integrating the ODE signaling network model with the stochastic cell spreading model.

The compartmental ODE model of signaling network was coupled with a three-dimensional stochastic model of cell spreading (21) to obtain an integrated model of cell spreading regulated by signaling (Figure 1 main text). Briefly, the spreading model is a stochastic spatio-temporal model of consisting of actin filament elongation, branching and capping reactions. The plasma plasma membrane physical properties are represented by surface load (p, $pN.\mu m^{-2}$) and bending rigidity (K_b, $pN.\mu m$). The spreading model is implemented in C++ using discrete differential geometry methods. The output from the ODE model was saved as a text file with active Arp2/3 and gelsolin and G-ATP-actin concentration as a function of time. The stochastic spreading model accepts model parameters, reactions and concentrations as input files and runs the Gillespie's algorithm for the actin filament elongation, branching and capping reactions. This model was modified to access a look-up table that was generated by the text file containing the levels of activated Arp2/3 and gelsolin and G-ATP-actin at every time step of the computation (using linear interpolation when necessary). The flowchart for the process is outlined in Figure 1B. The numerical simulations for the ODE model were run in the *Virtual Cell* suite and the concentrations of Arp2/3, gelsolin and G-ATP-actin were exported as text files. This text file is then used an input file to the spreading program. When the spreading model is initialized, it uses the parameters file to initialize the number of filaments (4000), the allowed reactions, kinetic parameters and the plasma membrane parameters (Table S3). Once this is initialized, the spreading model uses Gillespie's algorithm to compute the reaction rates and corresponding wait times. As the spreading model runs, at each time step, t, the concentrations of Arp2/3 gelsolin and G-actin are updated based on the text file from the multi-compartment ODE model of the signaling network (Figure 1B). The spreading model interpolates the concentrations linearly to obtain the concentrations at the exact time step for the Gillespie's algorithm.

Stochastic spatio-temporal model of cell spreading

This is a 3D model of actin filament growth constrained in a 0.2-μm region above the glass slide on which the cell spreads to conform with TIRF microscopy used to observe and quantify cell spreading. The conditions stated in Table S3 describe the initial status of a spreading cell: a spherical surface with 4000 evenly distributed actin filaments ready for growth. The reason why cell spreading model is constrained in a 0.2-μm region is that the actin dynamics at the leading edge of an isotropic spreading cell is thoroughly studied and this is the region that has active remodeling of the actin cytoskeleton during spreading. Our model does not attempt to simulate any parts other than the 0.2-μm thick leading edge of the spreading cell. Therefore, the volume of the spreading cell is not maintained constant as it should be in a study where the entire cell is explicitly modeled.

The structure of filament network, surface geometry of cell plasma membrane, and molecular concentrations are treated naturally in 3D, and no 2D or quasi-3D approximations are used. Since we assume that the leading edge of the spreading cell occurs only within a narrow 0.2-μm region above the glass slide, the model terminates the growth of all actin filaments that go beyond this region. This leads to a flat-disk appearance of the spreading cell.

During cell spreading, the absolute area of the plasma membrane surface at the leading edge increases as the leading edge protrudes outwards. Such area increase is realized by the removal of invaginations in the plasma membrane or fusion of inner plasma membrane reservoir to cell surface to meet the need of cell spreading. When uncapped filaments elongate and push the cell plasma membrane, the mechanical energy associated with the change of surface geometry is represented as change in surface curvature. This energy change regulates filament growth negatively and is incorporated as a feedback feature in our model, where change in energy becomes the negative regulator of reactions underlying filament growth. This energy change of cell plasma membrane is estimated by the work that actin filaments have to do in order to break and reform the surface. These concepts are implemented in the model using computational geometry methods linking the actin filament biochemistry to plasma membrane biophysics.

Biochemical Core of the Model

The spreading model consists of three filament reactions - filament elongation, filament branching and filament capping. These three reactions are based on the dendritic nucleation model and capture the fundamental dynamics of a growing filament network (15). The filament elongation reaction is modeled as the addition of an actin monomer to the barbed end of an existing filament, increasing the filament length by δ (Table S1). The branching reaction is mediated by Arp2/3 and the rate of branching reaction depends on the number of existing filaments, the availability of actin monomers and the Arp2/3 concentration. The filament branch occurs at a 70° angle to an existing filament.

$$G - ATP - actin + F - actin_n \xrightarrow{11.6} F - actin_{n+1}$$
$$2G - ATP - actin + F - actin_n \xrightarrow{1.22} F - actin_n + F - actin_2$$
$$CAP + F - actin_n \xrightarrow{35} F - actin_n - CAP$$

Local Plasma membrane Regulation of Cell Spreading:

The three actin filament remodeling reactions are modulated by the interaction of the cytoskeleton with the plasma plasma membrane. The elastic Brownian ratchet model proposed by Mogilner and Oster (22) is adapted in three dimensions to model the filament-plasma membrane interactions. The actual reaction velocity in the presence of a load is less that the reaction velocity for a freely growing filament without any resistance and is dependent on the probability that a gap of width (δ) is created between the filament tip and the load (in this case, the plasma membrane) (22). The modified rate constant is given by

$$k_{on}^{'} = k_{on} e^{\frac{-\Delta E}{k_B T}} \quad \text{- Eqn 1}$$

where ΔE is the energy change required to push the plasma membrane forward by a distance δ. ΔE is a local parameter and depends on the location of the growing filament and the area of the plasma membrane it is pushing. ΔE is computed as follows.

There are three main contributions to the energy change - plasma membrane surface energy, filament flexibility and the plasma membrane bending rigidity (23,24).

We treat the actin filaments as rigid filaments based on the assumption that filament bending undulations are much faster than the polymerization kinetics (22,25,26). We include two major contributions to the plasma membrane energy change - the plasma membrane surface energy and the plasma membrane bending energy.

The plasma membrane surface energy characterizes the work required by the filament to push an area dA (μm^2) of the plasma membrane forward to accommodate an actin monomer of length (δ=0.275nm). We characterize the plasma membrane surface resistance by a pressure p ($pN/\mu m^2$). this is the load offered by the plasma plasma membrane, similar to the definitions in (22,24,27). We use p=100 $pN/\mu m^2$ (22) as our control. The energy contribution from the plasma membrane surface term is given by

$$\Delta E_{surface} = pdA\delta \quad \text{- Eqn 2}$$

The other important contribution comes from plasma membrane bending. The plasma membrane bending rigidity is a physical property that characterizes the flexibility of the plasma membrane K_b ($pN.\mu m$). By incorporating this term, we are accounting for a bendable rather than rigid plasma membrane. The bending energy contribution is then given by

$$\Delta E_{bending} = K_b \int H^2 \, dA \quad \text{- Eqn 3}$$

where H is the local plasma membrane curvature (μm^{-1}). We use a value of K_b=0.08 $pN.\mu m$ (24).

Therefore, the net change in energy that affects the biochemical rates is

$$\Delta E = \Delta E_{bending} + \Delta E_{surface} \quad \text{- Eqn 4}$$

3.1 Interpolation and time steps

In order to ensure that the interpolation and the time interval of concentration input did not affect the spreading model, simulations were conducted with time intervals of the concentration profiles for 0.01 s and 1 s, 5 s and 10 s. The results of each condition were averaged over 24 simulations and show that the behavior is the same (Figure S5) and that the interpolation allows us to accurately read the concentrations of Arp2/3, gelsolin and G-ATP-actin over time. Thus, the time step in the text file input to the spreading model does not alter the spreading behavior simulated.

4. Model Assumptions and Simplifications

In developing the integrated modeling for signaling and spreading, some simplifying assumptions were made. Here we discuss these assumptions, the reasons for making them and the impact on the results if those assumptions are neglected. The assumptions were made with the proviso that if the output from the integrated model did not correlate with experimental observations of spreading, the model would be modified. Since the isotropic spreading behavior obtained from the integrated model was in good agreement with the observed experimental spreading behavior, the assumptions described here were retained and the model was not changed.

Integrin clustering and isoforms of subunits

Integrin clustering is an important phenomenon that regulates the unique aspect of integrin signaling – inside-out signaling and outside-in signaling (28,29). By means of this mechanism, integrins act not only as receptors responding to an extracellular stimulus but also as force transducers and substrate rigidity sensors. Additionally, these clusters also allow for the formation of nascent adhesion sites. These properties are important for motility processes. However, in this signaling model, integrins are treated as receptors. The reason for making this assumption is that the model focuses on the concentration profiles of activated Arp2/3, gelsolin and G-actin-ATP (via profilin activation). The mechanotransduction aspect of integrin signaling plays an important role in later phases of spreading, such as retraction and blebbing. In fact, once intiated,

isotropic spreading has been observed even in the absence of integrin mediated signaling (30,31). Therefore, this assumption is reasonable for modeling isotropic spreading.

Multiple GEFs and GAPs for Rho-GTPases and crosstalk between them

The signaling model does not account for the multiple guanine nucleotide exchange factors (GEFs) and GTPase activating proteins (GAPs) that are capable of maintaining the GTP-bound state for Rho, Rac and Cdc42. Many of the GEFs and GAPs are known to act on more than one small RhoGTPase (32). Including these interactions would make the signaling network more complex; however there is no current evidence that the shared GEFs or GAPs limit signal flow to one GTPase versus another. Hence it was assumed that this cross regulation, if it occurred, would not significantly affect spreading. The simulations supported this assumption and hence this simplifying assumption was not changed.

Spatial localization of signaling components

Many signaling proteins have spatially distinct patterns of activation. For example, Rho is more active at the trailing edge, and Rac at the leading edge (33-35). Models of this spatial segregation and of actin polymerization have been developed and highlight the role of location in actin remodeling (34,36). However, the resolution of this spatial localization is at a micron level or cellular scale (leading edge versus the trailing edge) rather than at the nanometer level of the lamellipodium width. Since the spreading model focuses on the stochastic remodeling of actin filaments at the leading edge we assumed that the spatial distribution of these components was uniform at the leading edge. It is possible that including the spatial variation of Arp2/3, gelsolin and G-ATP-actin along with diffusion capabilities will lead to a spatial variation in polymerization behavior. The main goal of developing this model is to obtain the dynamics of fast isotropic spreading. Since the radius maps for spreading behavior from the integrated model showed qualitatively similar dynamics in simulations experiments, we did not include the spatial dimension in signaling. Recent studies have begun to explore the

spatial aspect of actin polymerization (36) and as more details emerge, the current signaling model can extended to include this information.

Other actin reactions

In this spreading model, we have included only a subset of actin reactions. We have not included filament severing, depolymerization, annealing and bundling. All of these reactions are important for maintaining the structure of the cytoskeleton. However, since the model is based on the dendritic nucleation model of actin polymerization (37) and *in vitro* reconstitution experiments have established that a small subset of actin reactions is sufficient to capture motility behavior (15), we did not include the other reactions. Including these reactions will most likely change the relationships for the rate of actin polymerization and the filament size distribution. However, as we show later, the dynamics of polymerization are limited by the plasma membrane biophysical properties and including these reactions would most likely not have a large impact on the observed polymerization dynamics.

Filament bundling and actin filament rigidity

The interaction of actin filaments with the plasma plasma membrane was modeled using the elastic Brownian ratchet model (26). This is already a generalization of the Brownian ratchet model (38) to include the elasticity of the growing polymer. Therefore, we do not explicity include the filament elasticity in the plasma membrane energy requirements. While we include α-actinin in our signaling model for profilin activation, we do not include filament bundling in the spreading model. Filament bundling is mediated by α-actinin (39-41) and the elastic properties of a bundle of filaments may be different from a single filament depending upon bundle thickness. Filament bundling is an important event in filopodia formation and stress fiber formation. For the purposes of actin remodeling in the lamellipodia, where the filaments predominantly exhibit a branched network structure (42), we assumed that these interactions are not necessary to model fast isotropic spreading. Recently, Urban et al noted that in their experiments that the actin filaments at the leading edge may be predominantly unbranched (43). Future

models can incorporate this possibility as the molecular mechanisms underlying the growth and force-generation capabilities of unbranched actin networks are elucidated.

Unidirectional control from signaling to spreading

This model treats the output from the signaling network as an input to the spreading model, but there is no explicit effect of the spreading dynamics on the signaling model. It is also likely that the plasma membrane-imposed load will affect the dynamics of integrin signaling. This effect is modeled within the spreading model where plasma membrane forces control the actin remodeling reactions. The simplifying assumption of unidirectional control from signaling to spreading was made in order to keep the hybrid model computationally tractable. It is likely that a fully-integrated model of signaling and spreading would involve feedback from the spreading dynamics to signaling as well. In building a uni-directional model, we made the assumption that the changes to the signaling dynamics by the changing cell size and shape are not likely to be critically important. As the numerical simulations were conducted, testing of the predictions of the experiments and comparisons between experiments and simulations indicated that our simplifying assumption was valid. Further, the unidirectional information flow from the signaling model to actin filament cell spreading model is reasonable since for the time period of fast isotropic cell spreading, the change in cell size is not significant to change the volume of the cell in the juxtamembrane region and does not lead to large dilution effects on concentrations of signaling components. Plasma membrane area increases by exocytosis during later stages of spreading, but in isotropic spreading, the rearrangement comes from the plasma membrane folds and flattening of the cell on the surface (44).

5. Sensitivity of F-actin concentration to $k_{capping}$ and G-ATP-actin

The value of $k_{capping}$ was varied as 20, 35, 50 $\mu M^{-1}s^{-1}$ (the base value is 35 $\mu M^{-1}s^{-1}$). Decreasing the capping rate only slightly decreased the fold change in spreading radius and rate of polymerization (Figure S7A and C). The shape evolution did not depend on rate of capping reaction (Figure S7B).

The initial concentration of G-ATP-actin in the model was varied as 0, 5, 10, 15 μM (10 μM is the base value in the signaling model). When the initial concentration was set to zero, although the concentration of G-ATP-actin increased in response to signaling, spreading did not occur because of the low rates of polymerization (Figure S8C). The cell spreading size showed a dependence on the initial concentration of G-ATP-actin (Figure S8A) and there was a corresponding dependence on the rate of polymerization (Figure S8C). Spreading shape however did not change for the different G-ATP-actin concentrations (Figure S8B), suggesting that the compliance factor (Figure S7D, S8D) was a stronger controller of the shape evolution than G-ATP-actin or $k_{capping}$.

6. Role of individual components

In the simulations discussed in this section, the values of p and K_b are maintained at 100 pN/μm^2 and 0.08 pN. μm respectively.

6.1 Integrin receptors

When the signaling is turned off from the integrin receptors and the feedback feedback loops involving Arp2/3-Tiam 1 and Shp2 activation of Src were also turned off, there was no activation of Arp2/3 or gelsolin in the signaling network. The concentration of G-ATP-actin remains unchanged from the initial value of 10 μM (Figure S9A). This resulted in a condition where spreading did not occur. Integrin knockouts exhibit impaired spreading and motility behavior (45-48). In such systems, signals from integrin would be zero and there would be no basal activities in the down stream feedback loops. Hence in the simulations the feedback loops were also turned off.

Analysis of the maximum rates of polymerization (Figure S9B) shows that in the absence of signaling trigger, the rate of polymerization is at a constant low value (the only contributing term in equation for R_{free} in the main text is $k_{elongation}$[G-ATP-actin]). Because Arp2/3 is not activated and G-ATP-actin is at a low constant value, the initial steep increase in maximum rate of polymerization is missing in the absence of signaling.

This reiterates our finding that signaling network trigger is important for the initiation of isotropic spreading.

6.2 FAK knockout

Focal adhesion kinase is an important tyrosine kinase that is autophosphorylated in response to integrin activation. In the absence of FAK, the feedback loop with Csk and Src is disrupted. As a result, Src stays activated longer. FAK is also required for the activation of p190RhoGEF and Cdc42GAP. Further, Cdc42GAP is not activated resulting in longer and higher activation of Cdc42GTP and subsequent activation of WASP and Arp2/3. Therefore, in the absence of FAK, Arp2/3 activation is higher (Figure S6). Because the profilin/G-ATP-actin and the gelsolin loops are not directly by FAK, their activation is not affected to a large extent. The maximum rate of polymerization is similar at early times in the presence or absence of FAK. This results in a spreading behavior similar to that of control spreading behavior (Figure S10). The shape dynamics (circularity) are not affected by the changes in the signaling dynamics.

6.3 Src knockout

In the model, Src participates in the regulation of many components (Table S1). When no Src is available in the signaling network, many downstream components do not get activated. This results in a lower concentration of Arp2/3 and gelsolin being activated (Figure S11). For the Arp2/3 loop, the activity of Src is required for PIX/Cool activation. When there is no Src present, Cdc42 cannot be activated, therefore the only Arp2/3 activation comes from the Rac-WAVE pathway. Since WASP is not activated, there can be no activation of the WASP-PIX/COOL feedback loop. For gelsolin to be activated, Src is required for PLC-γ phosphorylation. The calcium dynamics from the ER to the cytoplasm in the absence of PLC-γ are at a basal level only, resulting in a low level of gelsolin activation (Figure S11). Absence of Src does not alter the G-ATP-actin levels, since this pathway is maintained by a series of binding events directly mediated by

integrin receptors. The maximum rate of polymerization is similar at early times for control and in the absence of Src and deviates at later times (Figure S11). However, the spreading behavior is similar in both cases; the differences in the dynamics of size and shape evolution are extremely small.

6.4 RPTP depletion

RPTP-α has been shown to be important in mechanotransduction of signals from the substrate to the actin cytoskeleton. In the signaling model, RPTP-α is important for signal transduction and maintaining the phosphorylated states of many components. The main activation step for RPTP-α comes from the integrin receptors directly. RPTP-α activation is limited also by a downstream loop coming from Rac. Depleting RPTP in the system by setting the initial concentration to zero leads to a decrease in the activation of Arp2/3 (Figure S12). Lack of RPTP disrupts Src activation and FAK activation. This results in low level signaling through the modules to Arp2/3. G-ATP-actin activation is not affected, but gelsolin activation is affected because of the low level of kinase signaling upstream (Figure S12). The maximum rate of polymerization is similar to that of the case where no Src is present (see Figure S12). The spreading behavior is again robust, showing no big changes between the control and the absence of RPTP-α.

6.5 Talin depletion

Setting the concentration of talin to zero changes the signaling dynamics of Arp2/3, gelsolin and G-ATP-actin. This is because talin plays an important role in the activation of PIP kinase type I γ. In its absence, PIP kinase type I γ activation is now entirely dependent on the priming events by RhoGTP and Cdc42GTP. The activation of PIP kinase type I γ by Cdc42 is limiting because the resulting synthesis of $PI(4,5)P_2$ by PIP kinase type I γ activation uses up $PI(4,5)P_2$ and Cdc42 for WASP activation. The absence of talin thus alters the balance of $PI(4,5)P_2$ synthesis in terms of timing and concentration. Since $PI(4,5)P_2$ is a key signaling component that directly impacts the

activation of the three actin remodeling proteins, altering the dynamics of $PI(4,5)P_2$ synthesis changes the dynamics of Arp2/3, gelsolin and G-ATP-actin activation (Figure S9). As a result, Arp2/3 activation is increased nearly two fold while gelsolin activation is decreased by half. While the concentration of G-ATP-actin does not change a lot, the dynamics are different. As a result, the maximum rate of polymerization is higher in the absence of talin at later times (Figure S13). Correspondingly, the cell spreading size is marginally larger in the absence of talin, but the shape dynamics is similar to that of control. The large differences in free rates of polymerization are translated into small changes in observed rates of polymerization because of the plasma membrane-imposed resistance to actin polymerization.

6.6 PIP kinase type I γ depletion

PIP kinase type I γ is required for the synthesis of $PI(4,5)P_2$ from PI(4)P. In the absence of PIP kinase type I γ, Arp2/3 activation is greatly diminished. The activation of Arp2/3 through the WAVE pathway is not as affected but the activation of WASP is decreased. The net result is a decreased activation of Arp2/3 (Figure S10). Gelsolin activation is also affected because of the lower levels of $PI(4,5)P_2$ in the system. G-ATP-actin and profilin activation are higher because the lower levels of $PI(4,5)P_2$ result in lower inactivation of α-actinin and profilin (Figure S14). The rate of polymerization is lower in the absence of PIPKI but the early values are similar. This rate of polymerization seems sufficient to initialize spreading. The shape dynamics are not affected by changes in the signaling dynamics (Figure S14).

6.7 PI(4)P depletion

The phosphatidylinositol phosphates control most of the regulation in this signaling network. In order to identify the role of PI(4)P in signaling, its initial concentration was set to zero. When PI(4)P is absent, $PI(4,5)P_2$ and $PI(3,4,5)P_3$ are available only in small quantities (PI(4)P is the most abundant of the three phospholipids

(49)). The removal of PI(4)P results in the same behavior as the absence of PIPKI. Arp2/3 activation and gelsolin activation are diminished and G-ATP-actin is slightly elevated (Figure S15). The size and shape evolution of the spreading cell show no changes during phase 1 spreading (Figure S15).

6.8 Cdc42 depletion

Cdc42 is a direct activator of N-WASP. When no Cdc42 is present, Arp2/3 activation is limited (Figure S6). Arp2/3 activation occurs by Rac activation of WAVE, which is unaffected by the absence of Cdc42. Gelsolin and G-ATP-actin dynamics are not affected. Therefore, absence of Cdc42 results in lowering the activation of Arp2/3 by about 10 fold compared to control (Figure S6). The dynamics of Cdc42 knockout or WASP inhibition are similar, the net effect on Arp2/3 is the same. In the absence of Cdc42, the spreading size is somewhat decreased but circularity does not change. This was a surprising effect but experiments with Cdc42DN and wiskostatin mediated inhibition of WASP showed similar results where phase 1 spreading was not affected (Figure S6). Recently, Nolen *et al.* noted that inhibition of Arp2/3 by Arp2/3 specific inhibitors did not alter keratocyte motility appreciably (50) and suggested that even small quantities of Arp2/3 are sufficient to maintain cell motility. Based on the analysis presented in the main text, the sensitivity parameters for branching are in fact not dependent on Arp2/3 concentration and G-ATP-actin may be the driving biochemical component. This combined with the role of plasma membrane-imposed resistance may allow for actin polymerization and spreading to occur during the isotropic phase.

6.9 PLC-γ depletion

Depletion of PLC-γ or calcium in the endoplasmic reticulum does not alter the kinetics of activation of Arp2/3 and G-ATP-actin. However, the activation of gelsolin is affected because the only calcium signal available is from the basal release and not by the active PLC-γ. This results in gelsolin activation that is about 15-fold lower than in control (Figure S16). Arp2/3 and actin dynamics are not affected. As a result the

spreading size is somewhat larger than control, with no change in circularity. These results are in agreement with experimental observations that PLC-γ null cells are still able to spread, suggesting that PLC-γ is not essential for spreading (51,20).

6.10 α-actinin depletion

α-actinin is required for the activation of profilin. When there is no α-actinin present in the system, profilin activation is diminished and therefore, G-ATP-actin concentration is also reduced (Figure S17). Interestingly Arp2/3 activation is increased in the absence of α-actinin. This is because $PI(4,5)P_2$ is no longer inactivating α-actinin and therefore, more $PI(4,5)P_2$ is available for Arp2/3 activation via Cdc42 and WASP. Comparing the rates of polymerization shows that the free rate of polymerization in the absence of α–actinin is lower than that of control (about 100 reactions per second). The observed rate of polymerization is similar for both cases indicating that the plasma membrane-imposed load is able to correct for the large differences in free rates of polymerization and allow for spreading behavior.

The only case where we were unable to obtain spreading behavior was when all the components in module 1 of the signaling network and the phosphatidylinositol lipid pathway (PI(4)P, $PI(4,5)P_2$, $PI(3,4,5)P_3$, PI3 kinase, PIP kinase type 1 g, FAK, Src, Shp2, Talin) were all set to zero.

Experimental observations in the literature on the role of various components

Activation of the Arp2/3 complex is regulated by multi-component complexes containing signaling proteins, phospholipids and cytoskeletal proteins (22). Phospholipids play an important role in regulating cytoskeleton interactions. $PI(4,5)P_2$, along with Cdc42 relieves the autoinhibition of N-WASP, which then activates the Arp2/3 complex (23).Similarly, WAVE is activated by Rac and $PI(3,4,5)P_3$ (24). The actin modulating proteins VASP, WASP, profilin and the Arp2/3 complex localize to the periphery of the protruding lamellipodia (25-27). Studies with knockouts of PLC-γ have revealed that at

low fibronectin concentration, the adhesion formation in fibroblasts is diminished. However, PLC-γ is not essential for spreading and adhesion but facilitates these functions (28). Similarly FAK (-/-) cells showed reduced migration speeds and increased focal adhesion formation, but the absence of FAK did not completely abolish cell migration (29). Src-deficient fibroblasts had deficiencies in adhesion formation and the initiation of spreading take longer in these cell (30). Thus, Src kinase is believed to play a role in regulating the focal adhesion location and turnover. Nevertheless even in the absence of Src, the fibroblasts were able to spread. Cdc42DN cells showed similar spreading kinetics to wild-type cells (31) during the isotropic phase.

Tables

Table S1: Reactions and Kinetic Parameters for Signaling Network

Module 1 for signaling network

	Name	Reference	Compartment	Nature	Kinetic Parameters	Reference	Notes
Integrin, FAK and Src activation							
1	Integrin + fibronectin => integrin*	(51,52)	Plasma Membrane	Binding	K_f=100 $\mu M^{-1}.s^{-1}$ K_b=0.168 s^{-1}	(53)	Integrin binding fibronectin
2	Integrin* + FAK => FAKp	(51,52)	Plasma Membrane	Binding	K_m=6.7 µM K_{cat}=0.9375 s^{-1}	(54)	FAK autophosphorylaton
3	FAKp + Shp2 => FAK	(55)	Cytoplasm	Enzymatic	K_m=1.7 µM K_{cat}=0.11 s^{-1}	(56)	FAK is inactivated by Shp2 by dephosphorylation
4	FAKp + Src => Src*	(51,52)	Plasma Membrane	Enzymatic	K_m=6.7 µM K_{cat}=0.9375 s^{-1}	(54)	FAK activation of Src
5	FAKp + Csk => Csk*	(51,52)	Cytoplasm	Enzymatic	K_m=6.7 µM k_{cat}=0.9375 s^{-1}	(54)	FAK activates Csk
6	Shp2+ Src => Src*	(57)	Plasma Membrane	Enzymatic	K_m=1.7 µM K_{cat}=0.11 s^{-1}	(56)	Shp2 activates Src
7	Csk* + Src* => Src	(51,52,57)	Plasma Membrane	Enzymatic	K_m= 4 µM K_{cat}=0.15 s^{-1}	(58)	Csk inactivates Src
8	Shp2 + Csk* => Csk	(57)	Cytoplasm	Enzymatic	K_m=1.7 µM K_{cat}=0.11s^{-1}	(56)	Shp2 dephosphorylates Csk
9	RPTP + Src => Src*	(57)	Plasma Membrane	Enzymatic	K_m=10 µM K_{cat}=0.11s^{-1}	(59)	Src is activated by RPTP
10	RPTP + Integrinbound => RPTP*	Assumed	Plasma membrane	Enzymatic	K_m=0.5 µM K_{cat}=0.2 s^{-1}	assumed	Activation of RPTP by activated integrins, based on the observations in

							(60)
11	RPTP* => RPTP	Assumed	Plasma Membrane	First order inactivation	K_f=1.0 s^{-1}	Assumed	Inactivation of RPTP

Module 2: Talin and PIPKI activation							
12	Talin + PIP2 => TalinPIP2	(61)	Plasma Membrane	Binding	K_f=1 $\mu M^{-1}.s^{-1}$ K_b=5 s^{-1}	Est	PIP2 binding activates Talin
13	Integrin* + TalinPIP2 => Talin*	(61)	Plasma Membrane	Binding	K_f=3.9 $\mu M^{-1}.s^{-1}$ K_b=2.1 s^{-1}	(62)	Ligand bound integrin activates Talin
14	Talin* + PIPKI => PIPKI*	(61)	Plasma Membrane	Binding	K_f=100 $\mu M^{-1}.s^{-1}$ K_b=17 s^{-1}	(61)	Activated Talin activates PIPKI
15	PIPKI* + Src* => PIPKIp	(63)	Plasma Membrane	Enzymatic	K_m=2.2 µM K_{cat}=0.025 s^{-1}	(64)	Src phosphorylates PIPKI (activation)
16	PIPKI* + FAKp => PIPKIp	(61)	Plasma Membrane	Enzymatic	K_m=6.7 µM K_{cat}=0.9375 s^{-1}	(54)	FAK phosphorylates PIPKI (activation)
17	PIPKIp + Shp1 => PIPKI	(63)	Plasma Membrane	Enzymatic	K_m=660 µM K_{cat}=1.063 s^{-1}	(65)	Shp1 inactivates PIPKI
18	PIPKI* + PI4P => PIP2	(63)	Plasma Membrane	Enzymatic	K_m=37 µM K_{cat}=0.19 s^{-1}	(66)	Synthesis of PIP2 by PIPKI This is the basal reaction; Assumption that the basal reaction has 10% of the activity of the activated reaction.
19	PIPKIp + PI4P => PIP2	(63)	Plasma Membrane	Enzymatic	K_m=37 µM K_{cat}=1.9 s^{-1}	(66)	Synthesis of PIP2 by PIPKI
20	PIP2 + Shp-1 => Shp-1 inactive	(1)	Plasma Membrane	Binding	K_f=0.1 $\mu M^{-1}.s^{-1}$ K_b=0.01s^{-1}	Est	PIP2 inactivates Shp1
21	PTEN + PIP3 => PIP2	(67)	Plasma Membrane	Enzymatic	K_m= 5 µM K_{cat}=0.006 s^{-1}	(67)	PTEN dephosphorylates PIP3
22	FAKp + PI3K => PI3K*	(51,52)	Plasma	Enzymatic	K_m=6.7 µM	(54)	FAK activates PI3K

			Membrane		K_{cat}=0.9375 s^{-1}		
23	PIP2 + PIP2ppase => PI4P	(68)	Plasma Membrane	Enzymatic	K_m=200 µM K_{cat}=640 s^{-1}	(68)	PIP2 is dephosphorylated by PIP2ppase
24	PIP2+PI3K* => PIP3	(69)	Plasma Membrane	Enzymatic	K_m = 50 µM K_{cat}=0.1433 s^{-1}	(70)	PIP3 synthesized by PI3Kinase
25	Shp2 + PI3K * => PI3K	Assumed	Plasma membrane	Enzymatic	K_m=1.7 µM K_{cat}=0.11s^{-1}	Assumed	PI3K inactivation

Module 3: RhoA activation							
26	FAKp + p190RhoGEF => p190RhoGEFp	(71)	Cytoplasm	Enzymatic	K_m=6.7 µM K_{cat}=0.9375 s^{-1}	(54)	FAK activates p190RhoGEF by phosphorylation
27	RhoGDP + p190RhoGEFp => RhoGTP	(71)	Plasma Membrane	Enzymatic	K_m=2.83 µM K_{cat} = 1s^{-1}	(72)	GEF activity
28	p190RhoGAPp + RhoGTP => RhoGDP	(57)	Plasma Membrane	Enzymatic	K_m=2.83 µM K_{cat}=0.99 s^{-1}	(73)	GAP activity
29	Shp2 + p190RhoGAPp => p190RhoGAP	(57)	Plasma Membrane	Enzymatic	K_m=1.7 µM K_{cat}=0.11 s^{-1}	(56)	Shp2 inactivates p190RhoGAP
30	Src* + p190RhoGAP => p190RhoGAPp	(57)	Plasma Membrane	Enzymatic	K_m=2.2 µM K_{cat}=0.025 s^{-1}	(64)	Src activates p190RhoGAP
31	RhoGTP => RhoGDP	(74)	Plasma Membrane	Intrinsic	K_f=0.02616s^{-1}	(75)	Intrinsic hydrolysis
32	RhoGTP + PIPKI => PIPKI*	(76)	Plasma Membrane	Binding	K_f=0.1 $\mu M^{-1}.s^{-1}$ K_b=0.01 s^{-1}	Est	Rho activates PIPKI
33	RPTP* + p190RhoGAPp => p190RhoGAP	(57)	Plasma Membrane	Enzymatic	K_m=10 µM K_{cat}=0.11 s^{-1}	(59)	RPTP inactivates RhoGAP
34	P160ROCK + RhoGTP => p160ROCK*	(69)	Plasma Membrane	Binding	K_f=10 $\mu M^{-1}.s^{-1}$ K_b=4290 s^{-1}	(77)	Rho Kinase activation by RhoGTP

35	P160ROCK* + RPTP* => p160ROCK	Assumed	Cytoplasm	Enzymatic	K_m=10 μM K_{cat}=0.11s^{-1}	(59)	Using RPTP to inactivate p160ROCK
36	p160ROCK* + PIPKI* => PIPKIp	(76)	Plasma Membrane	Enzymatic	K_m=2.2 μM K_{cat}=7 s^{-1}	(78)	Phosphorylation of PIPKI by p160ROCK

Module 4: Rac Activation							
37	Src* + p130Cas => p130Casp	(51,52)	Plasma Membrane	Enzymatic	K_m=2.2 μM K_{cat}=0.025s^{-1}	(64)	Src phosphorylates p130Cas and activates it
38	RPTP + p130Casp => p130Cas	(57)	Cytoplasm	Enzymatic	K_m=10 μM K_{cat}=0.11 s^{-1}	(59)	RPTP inactivates p130Cas
39	Shp1 + p130Casp => p130Cas	(79)	Cytoplasm	Enzymatic	K_m=660 μM K_{cat}=1.063 s^{-1}	(65)	Shp1 dephosphorylates p130Cas (inactivation reaction)
40	p130Casp + Crk => p130CaspCrk	(51,52)	Cytoplasm	Binding	K_f=1 $\mu M^{-1}.s^{-1}$ K_b=0.1s^{-1}	Est	P130Cas binds with Crk
41	Dock180Elmo + p130CaspCrk => Dock180Elmo *	(69)	Cytoplasm	Binding	K_f=1.0 $\mu M^{-1}.s^{-1}$ K_b=0.5 s^{-1}	Est	DockElmo is activated by Cas-Crk complex via binding
42	RhoGTP + Dock180Elmo => Dock180Elmo*	(80)	Plasma Membrane	Binding	K_f=1.0 $\mu M^{-1}.s^{-1}$ K_b=0.1 s^{-1}	Est	RhoGTP activates RacGEF DockElmo
43	Dock180Elmo* + RacGDP => RacGTP	(80)	Plasma Membrane	Enzymatic	K_m=1.35 μM K_{cat}=1 s^{-1}	(72)	GEF activity
44	PIP3 + Tiam1 => Tiam1*	(69)	Plasma Membrane	Binding	K_f=1 $\mu M^{-1}.s^{-1}$ K_b=0.1 s^{-1}	Est	PIP3 activates Tiam1, a RacGEF
45	RacGTP + PI3K => PI3K*	(69)	Plasma Membrane	Enzymatic	K_f=0.1 $\mu M^{-1}.s^{-1}$ K_b=0.01 s^{-1}	Est	Rac activates PI3K
46	Tiam1*+RacGDP => RacGTP	(69)	Plasma Membrane	Enzymatic	K_m=1.35 μM K_{cat}=1 s^{-1}	(72)	I assumed that Tiam1 has the same activity as p190RhoGEF for kinetic parameters.

47	RacGTP => RacGDP	(74)	Plasma Membrane	Intrinsic	K_f=0.050166s^{-1}	(75)	Intrinsic hydrolysis
48	RacGTP + RacGAP* => RacGDP	(73)	Plasma Membrane	Enzymatic	K_m=2.83 µM K_{cat}=0.99 s^{-1}	(73)	RacGAP activity. This reaction is formulated based on the similar reaction for p190RhoGAP and I used the same values as for p190RhoGAP
49	RacGAP + Src* => RacGAP*	assumed	Plasma Membrane	Enzymatic	K_m=2.2 µM K_{cat}=0.025s^{-1}	(64)	Src activates RacGAP
50	RacGTP + RPTP => RPTPinactive	(80)	Plasma Membrane	Binding	K_f=10 $\mu M^{-1}.s^{-1}$ K_b=1 s^{-1}	Est	RPTP is inactivated by RacGTP binding
51	RacGAP* + RPTP*=> RacGAP	Assumed	Plasma Membrane	Enzymatic	K_m=10 µM K_{cat}=0.11s^{-1}	(59)	Need to inactivate RacGAP

Module 5: Cdc42 Activation							
53	Src* + PIXCool => PIXCool*	(3)	Plasma Membrane	Enzymatic	K_m=2.2 µM K_{cat}=0.025 s^{-1}	(64)	PIXCool is activated by Src
54	PIXCool* + Cdc42GDP => Cdc42GTP	(3)	Plasma Membrane	Enzymatic	K_m=1.35 µM K_{cat}=2.3 s^{-1}	(72)	PIXCool is a Cdc42GEF
55	Cdc42GTP => Cdc42GDP	(74)	Plasma Membrane	Intrinsic	K_f=0.032 s^{-1}	(75)	Intrinsic hydrolysis
56	Cdc42GTP + Cdc42GAP* => Cdc42GDP	(81)	Plasma Membrane	Enzymatic	K_m=3.08 µM K_{cat}=1.52 s^{-1}	(81)	Cdc42GAP activity
57	Cdc42GAP + FAKp => Cdc42GAP*	Assumed	Plasma Membrane	Enzymatic	K_m=6.7 µM K_{cat}=0.9375 s^{-1}	(54)	Because Src activates PIX/Cool which is a Cdc42GEF, I used FAK to activate Cdc42GAP. This is based on the feedback nature of the Src and FAK and their interactions. (Balance)
58	Cdc42GAP*+ RPTP*=> Cdc42GAP	Assumed	Plasma	Enzymatic	K_m=10 µM	(59)	Cdc42GAP inactivation to balance

			membrane		K_{cat}=0.11s-1		Cdc42GAP activation
59	Cdc42GTP + PIPKI => PIPKI*	(76)	Plasma Membrane	Binding	K_f=0.1 $\mu M^{-1}.s^{-1}$ K_b=0.01 s^{-1}	Est	Cdc42 activates PIPKI

Module 6: Arp2/3 Module							
60	PIP3 + RacGTP + WAVE => WAVE*	(69)	Plasma Membrane	Binding	K_f=2.2X10^{-5} $\mu M^{-1}.s^{-1}$ K_b=1.65 s^{-1}	(82)	PIP3 and Rac activate WAVE. I used the same values as for WASP activation by PIP2 and Cdc42
61	WASP*+PIX/Cool => PIX/Cool*	(83)	Plasma Membrane	Binding	K_f=0.01 $\mu M^{-1}.s^{-1}$	Assumed	WASP activates PIX/Cool creating a Cdc42 feedback loop
62	WAVE* + Arp2/3 => Arp2/3*	(69)	Cytoplasm	Binding	K_f=10 $\mu M^{-1}.s^{-1}$	(7,84)	Arp2/3 activation by WAVE
63	PIP2 + Cdc42+ WASP => WASP*	(69,85)	Plasma Membrane	Binding	K_f=0.2 $\mu M^{-1}.s^{-1}$	(82)	PIP2 and Cdc42 activate WASP
64	WASP* + Arp2/3 => Arp2/3*	(69)	Cytoplasm	Binding	K_f=10 $\mu M^{-1}.s^{-1}$	(7,84)	Arp2/3 activation by WASP
65	Tiam1 + Arp2/3* => Tiam1*	(86)	Plasma Membrane	Bindng	K_f=10 $\mu M^{-1}.s^{-1}$ K_b=1 s^{-1}	Assumed	Tiam1 and Arp2/3 interaction links Rac activation to actin polymerization

Module 7: Gelsolin Module							
66	PIP2 + gelsolin =>gelsolin_inactive	(87-89)	Plasma Membrane	Binding	K_d = 20 μM K_f=1 $\mu M^{-1}.s^{-1}$ K_b=20 s^{-1}	(90)	PIP2 inactivates gelsolin (a capping protein) allowing actin filament elongation to occur.
67	Calcium + buffer ⇔ buffered_calcium	(91)	Cytoplasm	Binding	K_f=5.5 $\mu M^{-1}.s^{-1}$	(91)	Calcium concentration in the cytoplasm is kept low by the buffering protein
69	Calcium + gelsolin_inactive => gelsolin_active	(92)	Cytoplasm	Binding	K_f=0.1 $\mu M^{-1}.s^{-1}$	Est	Gelsolin is activated by calcium binding

70	PLCg+Src*=> PLCg*	(19)	Plasma membrane	Enzymatic	K_m=2.2 μM K_{cat}=0.025s^{-1}	(64)	PLCg is activated by Src
71	PIP2 + PLCγ* => DAG + IP3	(91)	Cytoplasm	Enzymatic	K_{cat}=0.1188 s^{-1}	(91)	PIP2 hydrolysis
72	PLCγ* => PLCγ	(91)	Cytoplasm	First order	K_f=0.2 s^{-1}	(91)	Inactivation of PLCg
73	DAG => degradation	(91)	Plasma membrane	First order	K_f=0.025 s^{-1}	(91)	Degradation of DAG
75	calciumER => Calcium	(93)	ER to cyto flux	Channel flux		(93)	This flux is taken from the paper by Loew and colleagues
76	PI3K + gelsolin* ⇔ PI3K*	(94)	Plasma membrane	Binding	K_f=0.01 $\mu M^{-1}.s^{-1}$ K_b=0.001 s^{-1}	assumed	PI3K is activated by gelsolin

Module 8: Profilin module							
77	Integrin* + α-actinin => α-actinin*	(95)	Plasma membrane	Binding	K_d=0.016 μM K_f=100 $\mu M^{-1}.s^{-1}$ K_b=1.6 s^{-1}	(95)	Ligand bound integrin activates α-actinin by binding
78	α-actinin* + zyxin => zyxin*	(95)	Cytoplasm	Binding	K_d=1.07 μM K_f=1 $\mu M^{-1}.s^{-1}$ K_b=0.00107 s^{-1}	(96)	Activated actinin can now bind to zyxin
79	α-actinin + PIP2 => α-actinin_inactive	(38)	Plasma membrane	Binding	K_d = 23 μM K_f=1 $\mu M^{-1}.s^{-1}$ K_b=23 s^{-1}	(38)	PIP2 binds to α-actinin and inhibits its activity
80	Zyxin* + VASP => VASP*	(97)	Cytoplasm	Binding	K_d=74 μM K_f=0.1 $\mu M^{-1}.s^{-1}$ K_b=0.0074 s^{-1}	(97)	VASP is activated by zyxin
81	VASP* +2 Profilin =>2 Profilin*	(98)	Cytoplasm	Enzymatic	K_d=84 μM K_f=10 $\mu M^{-1}.s^{-1}$ K_b=0.0084 s^{-1}	(98)	

82	PIP2 + profilin => profilinPIP2	(87,99)	Plasma Membrane	Binding	K_f=0.1 $\mu M^{-1}.s^{-1}$ K_b=0.01 s^{-1}	Estimated	Profilin is inactivated by PIP2 binding Use the same value for cofilin and profilin
83	PI3K + profilin* ⇔ PI3K*	(94)	Plasma membrane	Binding	K_f=0.01 $\mu M^{-1}.s^{-1}$ K_b=0.001 s^{-1}	Estimated	PI3K is activated by profilin
84	G-ADP-actin + profilin*=> G-ATP-actin	(100)	Cytoplasm	Binding	K_f=11.6* [profilin*] $\mu M^{-1}.s^{-1}$	(100)	Profilin binds to G-ADP actin and mediates the exchange of ADP to ATP.

Table S2: Initial Conditions

Number	Species	Compartment	Initial Concentration (units)	Notes	Reference
1	RhoGDP	Cytoplasm	0.5 μM	The value of Rho was measured as 34 ng/10^6 cells in COS1 cells. Conversion of this value to uM results in an approximate concentration of 1 uM per cell. The value chosen for our simulation is within that range and changing the initial concentration of RhoGDP did not alter the kinetics of Arp2/3, gelsolin and G-ATP-actin.	(101)
2	P190RhoGEF	Cytoplasm	0.01 μM	Assumed – varying the concentration of GEFs and GAPs in the signaling model did not significantly alter the dynamics of Arp2/3, gelsolin and G-ATP-actin activation.	
3	Shp1	Cytoplasm	0.1 μM	The concentration of Shp-1 ranges between 0.001-1% of total protein concentration depending on cell type. Assuming a total protein concentration of 300 g/l (102), the calculated concentration of Shp1 has an upper limit of 0.05 uM. Since the actual	(103)

				values are not known, we use a concentration of 0.1 uM.	
4	Csk	Cytoplasm	0.5 μM	Assumed to be similar to Src and FAK values. Variation of this concentration does not significantly alter the concentrations of Arp2/3, G-ATP-actin and gelsolin.	
5	WASP	Cytoplasm	9 μM		(85)
6	p130Cas	Cytoplasm	2 μM	Assumed - p130Cas is a scaffold protein whose intracellular concentration is not known. In our model, we assumed the initial concentration to be in the same range as that of other proteins that participate in binding reactions and complex formation (e.g.VASP)	
7	RacGDP	Cytoplasm	0.5 μM	The value of Rho was measured as 82 ng/10^6 cells in COS1 cells. Conversion of this value to uM results in an approximate concentration of 3 uM per cell. The value chosen for our simulation is within that range and changing the initial concentration of	

				RacGDP did not alter the kinetics of Arp2/3, gelsolin and G-ATP-actin.	
8	Tiam1	Membrane	20 molecules/μm^2	Assumed – varying the concentration of GEFs and GAPs in the signaling model did not significantly alter the dynamics of Arp2/3, gelsolin and G-ATP-actin activation.	
9	RPTP	Membrane	50 molecules/μm^2	Assumed – variation of the initial concentration of RPTP does not significantly alter the kinetics of Arp2/3, G-ATP-actin and gelsolin.	
10	Crk	Cytoplasm	0.1 μM	Assumed	
11	Talin	Cytoplasm	2 μM	Assumed –Talin is a scaffold protein whose intracellular concentration is not known. In our model, we assumed the initial concentration to be in the same range as that of other proteins that participate in binding reactions and complex formation (e.g.VASP)	
12	Cdc42GDP	Cytoplasm	0.5 μM	The value of Cdc42 was measured as 26 ng/10^6 cells in COS1 cells. Conversion of this value to uM results in an approximate concentration of 1	(101)

				μM per cell. The value chosen for our simulation is within that range and changing the initial concentration of Cdc42 GDP did not alter the kinetics of Arp2/3, gelsolin and G-ATP-actin.	
13	P160ROCK	Cytoplasm	0.1 μM	Assumed	
14	FAK	Cytoplasm	0.5 μM	Assumed – We assumed that the amount of FAK in a cell was similar to the amount of Src and calculated the concentration using number of molecules as 4 X 10^5 per cell in a volume of approximately 1500 um^3.	
15	Shp2	Cytoplasm	0.1 μM	Assumed to be the same as Shp1	
16	PIPKI	Cytoplasm	0.1 μM	This value was assumed. Variation of initial concentration of PIPKI affected only Arp2/3 kinetics. But the rate of polymerization and spreading behavior was not affected.	
17	Dock/Elmo	Cytoplasm	0.01 μM	Assumed – varying the concentration of GEFs and GAPs in the signaling model did not significantly alter the dynamics of Arp2/3, gelsolin and G-ATP-actin activation.	

18	Arp2/3	Cytoplasm	10 μM		(104)
19	WAVE	Cytoplasm	9 μM	Assumed to be the same as WASP concentration	
20	Profilin	Cytoplasm	5 μM		(99)
21	Fibronectin	ECM as density	50 molecules/μm^2	Fibronectin concentration used in spreading experiments was 6.6 mg/ml on a 3.1 cm^2 surface – This corresponds to a density of 5.83 X 10^{19} molecules/μm^2 on the surface. Therefore the assumption is that fibronectin concentration is greater than the density of integrin receptors and is not limiting.	(105)
22	PI4P	Membrane	15000 molecules/μm^2		(48)
23	P190RhoGAP	Membrane	100 molecules/μm^2	Assumed – varying the concentration of GEFs and GAPs in the signaling model did not significantly alter the dynamics of Arp2/3, gelsolin and G-ATP-actin activation.	
24	PIP3	Membrane	100 molecules/μm^2		(48)
25	Src	Membrane	200 molecules/μm^2	The number of Syk molecules per cell is measured as approximately 4 X 10^5 molecules per cell; using a surface area of 2000 μm^2 gives us an estimate for the molecular density of Src.	(106)
26	Srcactive	Membrane	0 molecules/μm^2	Active	

				concentrations of src are set to zero in the model.	
27	RacGTP	Membrane	0 molecules/μm^2	Assumed	
28	PI3K	Membrane	100 molecules/μm^2	Assumed – variation of this value did not change the kinetics of Arp2/3, gelsolin and G-ATP-actin kinetics	
29	Integrin	Membrane	36 molecules/μm^2	The density of integrins is about 180 molecules/μm^2, because I am only modeling the leading edge, which is about 20% of the total cell volume, I reduce the integrin density to 20%. Adhesion complexes have a higher density of integrins.	(107)
30	RacGAP	Membrane	100 molecules/μm^2	Assumed – varying the concentration of GEFs and GAPs in the signaling model did not significantly alter the dynamics of Arp2/3, gelsolin and G-ATP-actin activation.	
31	PIP2ppase	Membrane	100 molecules/μm^2	Assumed to be in the same range as PI3K	
32	PIP2	Membrane	500 molecules/μm^2		(48)
33	PIX/Cool	Membrane	100 molecules/μm^2	Assumed – varying the concentration of GEFs and GAPs in the signaling model did not significantly alter the dynamics of Arp2/3, gelsolin and G-ATP-actin	

				activation.	
34	Cdc42GAP	Membrane	100 molecules/μm^2	Assumed – varying the concentration of GEFs and GAPs in the signaling model did not significantly alter the dynamics of Arp2/3, gelsolin and G-ATP-actin activation.	
35	PLC-γ	Membrane	100 molecules/μm^2		(48)
36	Buffer	Cytoplasm	0.2 μM		(93)
37	Calcium	ER	200 μM		(93)
38	IP3	ER membrane	10 molecules/μm^2		(93)
39	Gelsolin (capping protein)	Cytoplasm	1 μM	Gelsolin concentration varies from 0.2-2 μM	(90,108)
40	VASP	Cytoplasm	2 μM		(108)
41	Zyxin	Cytoplasm	2 μM	Assumed same as VASP	
42	Alpha-actinin	Cytoplasm	2 μM	Assumed same as VASP	
43	G-ADP-actin	Cytoplasm	20 μM	Actin in ADP and ATP bound forms is present in large quantities (10- 100 μM)	(109)
44	G-ATP-actin	Cytoplasm	10 μM	This was used as a baseline value. Concentration of G-ATP-actin initial was varied in simulations.	

Table S3: Parameters used in the spreading model

No.	Parameter	Value	Units	References
1	**Rate constant of filament polymerization**	11.6	$\mu M^{-1}s^{-1}$	(100)
2	**Diameter of Actin Monomer** Although the diameter of individual actin monomer is 6 nm, the distance between neighboring actin monomers in actin filament is 5.5 nm due to the double helix structure of polymerized actin filament (110). Since the purpose of using this parameter is to determine the length increment of actin filament caused by filament polymerization reaction, the model assumes the diameter of actin monomer to be 5.5 nm. During an elongation reaction, the increase in the filament length d=2.75 nm.	5.5	nm	(110)
3	**Diameter of Arp2/3 protein** High-resolution experiment reveals the crystal structure of Arp2/3 protein complex and determines its dimensional size around 7 to 15 nm (111). The model uses the 15 nm as the diameter of Arp2/3 protein.	15	nm	(111)
4	**Diameter of capping protein** The diameter of capping protein is not known yet and must be estimated. Since capping protein is known to be a small molecule, the model assumes that it is smaller than Arp2/3 protein. And because capping protein can bind to the barbed end of double-helix actin filament, it implies that capping protein should be able to cover the size of two actin monomers. Therefore, the model assumes that the diameter of capping protein is 10 nm.	10	nm	Estimated
5	**Filament branching angle**	70°		(112)
6	**Number of nucleated monomers** This is the number of polymerized actin monomer in the initial actin filament nucleated by Arp2/3 protein in filament branching reaction. Based on the subunit structure of Arp2/3 protein, previous study suggests that the binding of two actin monomers to Arp2/3 protein be the initial step of creating a new actin filament (113).	2		(113)
7	**Number of monomers binding Arp2/3** This parameter describes the number of polymerized actin monomers on an existing filament that bind Arp2/3 during filament branching. (114) shows that the binding site of Arp2/3 on the existing filament covers about 6 to 7 polymerized actin monomers.	7		(114)
8	**Surface load from membrane** This is the average resistance force imposed on growing actin filament by unit area of cell membrane. This parameter is estimated from previous computational study (24) where the resistance pressure used ranges from 50 to 200 pN/μm on a 0.17-μm thick lamellipodium which corresponds to 300 to 1100 $pN/\mu m^2$. Because fibroblast cell is capable of buffering this resistance force with membrane reservoir during cell spreading (115), the model selects a constant intermediate value 100 $pN/\mu m^2$ for membrane resistance pressure.	100	$pN\ \mu m^{-2}$	(24)

9	**Membrane Bending Rigidity** We use the value of membrane bending coefficient as used in this model (23).	0.08	pN. μm	(23)
10	**Thickness of the leading edge** For the fast membrane protrusion involved in cell spreading or cell migration, the leading edge of cell membrane is usually like a flatted sheet and its thickness has been well measured (116).	200	nm	(116)
11	**Initial cell diameter** The value of this parameter is estimated directly from experiments where single fibroblast cell has spherical shape before it is dropped onto the glass slide coated with fibronectin signaling molecules. The initial diameter of spherical fibroblast cell is about a few microns before it starts spreading on glass slide. So the model assumes the initial cell diameter to be 2 μm.	2	μm	Estimated from experiment
12	**Thickness of the cortical region** The filament network at the very leading edge is cross-linked by highly branched and short filaments whereas the filament network inside cell is usually formed by straight and long filaments (117). Since this model only studies the actin dynamics of branched filament network, the model confines all filament reactions within the 50-nm cortical region underneath cell membrane.	50	nm	Estimated
13	**Initial number of actin filaments** The initial filament density was chosen so that it would be sufficient to initiate cell spreading. After being tested with various values, we decided to use 2000 actin filaments evenly distributed on spherical cell as the starting point of cell spreading simulation.	4000		Estimated
14	**Thermodynamic constant k_BT** Calculated at 300 K, where k_B is the Boltzmann constant	4.1	pN.nm	Calculated
15	**Rate constant of filament branching** Because of the highly branched structure of filament network at the leading edge of spreading cell, filament branching reaction is known to be very fast during cell spreading process. Since filament branching reaction is a fourth-order reaction and the concentration of actin monomer is assumed as 20 μM, the model selects 1.25 $\mu M^{-3} \cdot s^{-1}$ as the rate constant of filament branching reaction such that the reaction rate remains moderately high (ranges between 10 to 100 reactions per second).	1.25	$\mu M^{-3} s^{-1}$	Estimated
16	**Rate constant of filament capping** Since the binding affinity of capping protein to the barbed end of actin filament is known to be high and the rate of filament capping reaction should match the rate of branching reaction during cell spreading, the model assumes the rate constant of capping reaction to be 35 $\mu M^{-1} \cdot s^{-1}$ such that the rate of capping reaction is comparable with but a little smaller than the rate of branching reaction (ranges between 0.35 to 70 reactions per second).	35	$\mu M^{-1} s^{-1}$	Estimated

Table S4: Components that flux between compartment

Name	From Compartment	Name	To Compartment
Calcium	ER	Calcium	Cytoplasm
Cdc42GDP	Cytoplasm	Cdc42GTP	Plasma membrane
Dock/Elmo	Cytoplasm	Dock/Elmo active	Plasma membrane
Shp-1	Cytoplasm	Shp-1 inactive	Plasma membrane
PIPKI	Cytoplasm	PIPKIp (active)	Plasma membrane
RacGDP	Cytoplasm	RacGTP	Plasma membrane
RhoGDP	Cytoplasm	RhoGTP	Plasma membrane
Talin	Cytoplasm	Talin active	Plasma membrane

Figure Legends

Figure S1: Modules in the signaling network

The signaling network comprises eight modules regulating the activities of the actin regulating proteins Arp2/3, gelsolin and profilin. Module 1 focuses on integrin-fibronectin interaction and subsequent activation of FAK, Src and RPTP and their regulation by Shp-2 and Csk. Module 2 introduces talin, PIP kinase type I g and the lipid pathway. Modules 3-5 focus on the small RhoGTPases Rho, Rac and Cdc42 and the role of their respective guanine nucleotide exchange factor and GAPs. Module 6 is the activation of Arp2/3 by WASP and WAVE, module 7 focuses on gelsolin activation by calcium signaling and the balance by $PI(4,5)P_2$ inactivation. Module 8 shows the activation of profilin by a-actinin, zyxin and VASP. $PI(4,5)P_2$ provides the balance by inactivating a-actinin and profilin. Activated profilin allows for ATP exchange on G-ADP-actin, resulting in an increase in G-ATP-actin concentration.

Figure S2: Integrin signaling network

The modules described in Figure S1 together form the signaling network from integrins to the regulators of actin – Arp2/3, gelsolin and profilin.

Figure S3: Flowchart of the procedure used to compare experimental and simulation time course profiles for signaling components

The concentration profiles of key components in the signaling network were validated against kinetics of activation from the literature. The graph from the literature shown on the top left is converted into tabular form using ImageJ software's measurement tools. The data is then normalized to the maximum concentration. The data from simulation is used for the same time points and normalized. Comparison is made between the normalized dynamic profiles.

Figure S4: Comparison of the experimental and simulated activation kinetics of some components in the signaling network

In order to validate the time scales in the signaling network, comparison of the simulated activation profiles of six components in the signaling network with experimental measurements from the literature are shown. The experiments for Src activation kinetics (17) and FAK activation kinetics (17) were conducted using fibroblasts spreading on fibronectin coated surfaces. PLC-γ phosphorylation by Src (20) was conducted in an experimental setting with fibroblasts spreading on Matrigel. Rho and Rac activation profiles were obtained for integrin-stimulated Rho and Rac activation at the immunological synapse (19). The kinetics of p130Cas phosphorylation by Src was obtained from (18), where fibroblasts were used to study integrin stimulation by fibronectin. The original experimental data was extracted from the images in the papers using ImageJ and normalized concentrations were compared to simulation data. Concentrations were normalized by dividing all the values by the maximum value within that time course.

Figure S5: Varying the time steps to the input files does not alter calculations in the spreading model

Four different different time steps (0.01s, 1 s, 5 s, and 10 s) in the input concentration file were compared and found that the linear interpolation step introduced during integration of the ODE model with the stochastic spreading model did not alter the spreading behavior. The results shown are an average of 24 simulations for each time step.

Figure S6: Isotropic spreading behavior in the absence of Cdc42 and WASP

(A) Concentration profiles of (i) Arp2/3, (ii) gelsolin and (iii) G-ATP-actin when the initial concentration of Cdc42 or WASP is set to zero; (iv) Maximum rate of polymerization in reactions per second as expected from the signaling network alone.

(B) Spreading behavior and rates of polymerization using these concentration show that there is not much change from the control spreading behavior. (i) Radius map, (ii) velocity map, (iii) fold change in radius, (iv) circularity, (v) observed rate of polymerization and (vi) compliance factor.

Figure S7: Effect of Variation of $k_{capping}$ on isotropic cell spreading

The value of $k_{capping}$ was varied to test the sensitivity of F-actin to these values. Increasing $k_{capping}$ only slightly decreased cell spreading radius while cell shape was not affected. (A) Rate of polymerization, (B) Fold change in radius, (C) Circularity and (D) Compliance factor.

Figure S8: Variation of G-ATP-actin on isotropic cell spreading

The value of G-ATP-actin initial concentration was varied to test the sensitivity of F-actin to these values. Increasing G-ATP-actin decreased cell spreading radius while cell shape was not affected. (A) Rate of polymerization, (B) Fold change in radius, (C) Circularity and (D) Compliance factor. The G-ADP-actin initial concentration was maintained at 20 μM.

Figure S9: Spreading behavior in the absence of integrin receptors

(A) Concentration profiles of (i) Arp2/3, (ii) gelsolin and (iii)G-ATP-actin when the initial concentration of integrin receptors is set to zero and the feedback loops are turned off; (iv) Maximum rate of polymerization in reactions per second as expected from the signaling network alone. Arp2/3 and gelsolin are not activated in the absence of signaling trigger and G-ATP-actin remains at a constant value of 10 μM. When all basal activity is turned off in the signaling network, the spreading model cannot compute any filament reactions because the input is zero, a situation that we can regard as spreading failed to occur.

Figure S10: Spreading behavior in the absence of focal adhesion kinase in the signaling network

(A) Concentration profiles of (i) Arp2/3, (ii) gelsolin and (iii) G-ATP-actin when the initial concentration of focal adhesion kinase is set to zero; (iv) Maximum rate of polymerization in reactions per second as expected from the signaling network alone.

(B) Spreading behavior and rates of polymerization using these concentration show that there is not much change from the control spreading behavior. (i) Radius map, (ii)

velocity map, (iii) fold change in radius, (iv) circularity, (v) observed rate of polymerization and (vi) compliance factor.

Figure S11: Spreading behavior in the absence of Src kinase in the signaling network

(A) Concentration profiles of (i) Arp2/3, (ii) gelsolin and (iii) G-ATP-actin when the initial concentration of Src kinase is set to zero. (iv) Maximum rate of polymerization in reactions per second as expected from the signaling network alone.

(B) Spreading behavior and rates of polymerization using these concentration show that there is not much change from the control spreading behavior. (i) Radius map, (ii) velocity map, (iii) fold change in radius, (iv) circularity, (v) observed rate of polymerization and (vi) compliance factor.

Figure S12: Spreading behavior in the absence of RPTP in the signaling network

(A) Concentration profiles of (i) Arp2/3, (ii) gelsolin and (iii) G-ATP-actin when the initial concentration of RPTP is set to zero. (iv) Maximum rate of polymerization in reactions per second as expected from the signaling network alone.

(B) Spreading behavior and rates of polymerization using these concentration show that there is not much change from the control spreading behavior. (i) Radius map, (ii) velocity map, (iii) fold change in radius, (iv) circularity, (v) observed rate of polymerization and (vi) compliance factor.

Figure S13: Spreading behavior in the absence of talin

(A) Concentration profiles of (i) Arp2/3, (ii) gelsolin and (iii) G-ATP-actin when the initial concentration of Talin is set to zero. (iv) Maximum rate of polymerization in reactions per second as expected from the signaling network alone.

(B) Spreading behavior and rates of polymerization using these concentration show that there is not much change from the control spreading behavior. (i) Radius map, (ii) velocity map, (iii) fold change in radius, (iv) circularity, (v) observed rate of polymerization and (vi) compliance factor.

Figure S14: Spreading behavior in the absence of PIPKI

(A) Concentration profiles of (i) Arp2/3, (ii) gelsolin and (iii) G-ATP-actin when the initial concentration of PIP kinase type I γ is set to zero. (iv) Maximum rate of polymerization in reactions per second as expected from the signaling network alone.

(B) Spreading behavior and rates of polymerization using these concentration show that there is not much change from the control spreading behavior. (i) Radius map, (ii) velocity map, (iii) fold change in radius, (iv) circularity, (v) observed rate of polymerization and (vi) compliance factor.

Figure S15: Spreading behavior in the absence of PI(4)P

(A) Concentration profiles of (i) Arp2/3, (ii) gelsolin and (iii) G-ATP-actin when the initial concentration of PI(4)P is set to zero. (iv) Maximum rate of polymerization in reactions per second as expected from the signaling network alone.

(B) Spreading behavior and rates of polymerization using these concentration show that there is not much change from the control spreading behavior. (i) Radius map, (ii) velocity map, (iii) fold change in radius, (iv) circularity, (v) observed rate of polymerization and (vi) compliance factor.

Figure S16: Spreading behavior in the absence of PLC-γ

(A) Concentration profiles of (i) Arp2/3, (ii) gelsolin and (iii) G-ATP-actin when the initial concentration of PLC-γ is set to zero. (iv) Maximum rate of polymerization in reactions per second as expected from the signaling network alone.

(B) Spreading behavior and rates of polymerization using these concentration show that there is not much change from the control spreading behavior. (i) Radius map, (ii) velocity map, (iii) fold change in radius, (iv) circularity, (v) observed rate of polymerization and (vi) compliance factor.

Figure S17: Spreading behavior in the absence of α-actinin

(A) Concentration profiles of (i) Arp2/3, (ii) gelsolin and (iii) G-ATP-actin when the initial concentration of α-actinin is set to zero. (iv) Maximum rate of polymerization in reactions per second as expected from the signaling network alone.

(B) Spreading behavior and rates of polymerization using these concentration show that there is not much change from the control spreading behavior. (i) Radius map, (ii) velocity map, (iii) fold change in radius, (iv) circularity, (v) observed rate of polymerization and (vi) compliance factor.

Figure S18: Effects of variation of the physical properties of the plasma plasma membrane on simulated cell spreading characteristics

(A) Spreading behavior with K_b=0 pN. μm, varying p (0, 100, 500 pN. μm^{-2}). The plasma membrane surface resistance was varied (p=0, 100, 500) with K_b=0 pN.μM. The spreading size is smaller for larger p (panel A(i)), but the spreading shape continues to be non-circular (panel A(ii)) for all conditions.

(B) Spreading behavior with K_b=0.08 pN. μm, varying p (0, 100, 500 pN. μm^{-2}) The plasma membrane surface resistance was varied (p=0, 100, 500) with

K_b=0.08. The spreading size is smaller for larger p (panel B(i)), and the spreading shape is circular for all conditions (panel B(ii)).

(C) Spreading behavior with K_b=0.2 pN. μm, varying p (0, 100, 500 pN. μm^{-2})
The plasma membrane surface resistance was varied (p=0, 100, 500) with K_b=0.2. The spreading size is smaller for larger p (panel C(i)) and also smaller compared to panels Ai and Bi; the spreading shape is circular for all conditions (panel C(ii)).

References

1. Parsons, J. T., K. H. Martin, J. K. Slack, S. A. Boerner, and C. C. Martin. 2005. Integrin Signaling Pathway. Sci. Signal. (Connections Map in the Database of Cell Signaling).

2. Bairstow, S. F., K. Ling, and R. A. Anderson. 2005. Phosphatidylinositol phosphate kinase type Igamma directly associates with and regulates Shp-1 tyrosine phosphatase. J Biol Chem 280:23884-23891.

3. Ling, K., R. L. Doughman, A. J. Firestone, M. W. Bunce, and R. A. Anderson. 2002. Type I gamma phosphatidylinositol phosphate kinase targets and regulates focal adhesions. Nature 420:89-93.

4. Peterson, J. R. and J. Chernoff. 2006. Src transforms in a Cool way. Nat Cell Biol 8:905-907.

5. Mahaffy, R. E. and T. D. Pollard. 2006. Kinetics of the formation and dissociation of actin filament branches mediated by Arp2/3 complex. Biophys J 91:3519-3528.

6. May, R. C., M. E. Hall, H. N. Higgs, T. D. Pollard, T. Chakraborty, J. Wehland, L. M. Machesky, and A. S. Sechi. 1999. The Arp2/3 complex is essential for the actin-based motility of Listeria monocytogenes. Curr Biol 9:759-762.

7. Mullins, R. D., J. A. Heuser, and P. T. D. 1998. The interaction of Arp2/3 complex with actin: nucleation, high affinity pointed end capping, and formation of branching networks of filaments. Proc. Natl. Acad. Sci. 95:6181-6186.

8. Rohatgi, R., H. Y. Ho, and M. W. Kirschner. 2000. Mechanism of N-WASP activation by CDC42 and phosphatidylinositol 4, 5-bisphosphate. J Cell Biol 150:1299-1310.

9. Eden, S., R. Rohatgi, A. V. Podtelejnikov, M. Mann, and M. W. Kirschner. 2002. Mechanism of regulation of WAVE1-induced actin nucleation by Rac1 and Nck. Nature 418:790-793.

10. Alberts, B., A. Johnson, J. Lewis, M. Raff, K. Roberts, and P. Walter. 2002. Molecular Biology of the Cell: Garland Science. 1616 p.

11. Janmey, P. A., K. Iida, H. L. Yin, and T. P. Stossel. 1987. Polyphosphoinositide micelles and polyphosphoinositide-containing vesicles dissociate endogenous gelsolin-actin complexes and promote actin assembly from the fast-growing end of actin filaments blocked by gelsolin. J Biol Chem 262:12228-12236.

12. Kinosian, H. J., J. Newman, B. Lincoln, L. A. Selden, L. C. Gershman, and J. E. Estes. 1998. Ca2+ regulation of gelsolin activity: binding and severing of F-actin. Biophys J 75:3101-3109.

13. Janmey, P. A. and T. P. Stossel. 1989. Gelsolin-polyphosphoinositide interaction. Full expression of gelsolin-inhibiting function by polyphosphoinositides in vesicular form and inactivation by dilution, aggregation, or masking of the inositol head group. J Biol Chem 264:4825-4831.

14. www.vcell.org. Virtual Cell.

15. Loisel, T. P., R. Boujemaa, D. Pantaloni, and M. F. Carlier. 1999. Reconstitution of actin-based motility of Listeria and Shigella using pure proteins. Nature 401:613-616.

16. Pantaloni, D., C. Le Clainche, and M. F. Carlier. 2001. Mechanism of actin-based motility. Science 292:1502-1506.

17. Zhang, X., G. Jiang, Y. Cai, S. J. Monkley, D. R. Critchley, and M. P. Sheetz. 2008. Talin depletion reveals independence of initial cell spreading from integrin activation and traction. Nat Cell Biol.

18. Nojima, Y., N. Morino, T. Mimura, K. Hamasaki, H. Furuya, R. Sakai, T. Sato, K. Tachibana, C. Morimoto, Y. Yazaki, and et al. 1995. Integrin-mediated cell adhesion promotes tyrosine phosphorylation of p130Cas, a Src homology 3-containing molecule having multiple Src homology 2-binding motifs. J Biol Chem 270:15398-15402.

19. Makrogianneli, K., L. M. Carlin, M. D. Keppler, D. R. Matthews, E. Ofo, A. Coolen, S. M. Ameer-Beg, P. R. Barber, B. Vojnovic, and T. Ng. 2009. Integrating receptor signal inputs that influence small Rho GTPase activation dynamics at the immunological synapse. Mol Cell Biol 29:2997-3006.

20. Jones, N. P., J. Peak, S. Brader, S. A. Eccles, and M. Katan. 2005. PLCgamma1 is essential for early events in integrin signalling required for cell motility. J Cell Sci 118:2695-2706.

21. Xiong, Y., P. Rangamani, M. A. Fardin, A. Lipshtat, B. J. Dubin-Thaler, O. M. Rossier, M. P. Sheetz, and R. Iyengar. 2010. Mechanisms controlling cell size and shape during isotropic cell-spreading. Biophys J 98:2136-2146.

22. Mogilner, A. and G. Oster. 2003. Force generation by actin polymerization II: the elastic ratchet and tethered filaments. Biophys J 84:1591-1605.

23. Maly, I. V. and G. G. Borisy. 2001. Self-organization of a propulsive actin network as an evolutionary process. Proc Natl Acad Sci 98:11324-11329.

24. Schaus, T. E., E. W. Taylor, and G. G. Borisy. 2007. Self-organization of actin filament orientation in the dendritic-nucleation/array-treadmilling model. Proc Natl Acad Sci U S A 104:7086-7091.

25. Mogilner, A. and L. Edelstein-Keshet. 2002. Regulation of actin dynamics in rapidly moving cells: a quantitative analysis. Biophys J 83:1237-1258.

26. Mogilner, A. and G. Oster. 1996. Cell motility driven by actin polymerization. Biophys J 71:3030-3045.

27. Boal, D. 2002. Mechanics of the Cell. Cambridge: Cambridge University Press.

28. DeMali, K. A., K. Wennerberg, and K. Burridge. 2003. Integrin signaling to the actin cytoskeleton. Curr Opin Cell Biol 15:572-582.

29. Giancotti, F. G. and E. Ruoslahti. 1999. Integrin signaling. Science 285:1028-1032.

30. Cuvelier, D., M. Thery, Y. S. Chu, S. Dufour, J. P. Thiery, M. Bornens, P. Nassoy, and L. Mahadevan. 2007. The universal dynamics of cell spreading. Curr Biol 17:694-699.

31. Dubin-Thaler, B. J., J. M. Hofman, Y. Cai, H. Xenias, I. Spielman, A. V. Shneidman, L. A. David, H. G. Dobereiner, C. H. Wiggins, and M. P. Sheetz. 2008. Quantification of cell edge velocities and traction forces reveals distinct motility modules during cell spreading. PLoS One 3:e3735.

32. Schmidt, A. and A. Hall. 2002. Guanine nucleotide exchange factors for Rho GTPases: turning on the switch. Genes Dev. 16:1587-1609.

33. Machacek, M., L. Hodgson, C. Welch, H. Elliott, O. Pertz, P. Nalbant, A. Abell, G. L. Johnson, K. M. Hahn, and G. Danuser. 2009. Coordination of Rho GTPase activities during cell protrusion. Nature 461:99-103.

34. Dawes, A. T. and L. Edelstein-Keshet. 2007. Phosphoinositides and Rho proteins spatially regulate actin polymerization to initiate and maintain directed movement in a one-dimensional model of a motile cell. Biophys J 92:744-768.

35. Kurokawa, K., T. Nakamura, K. Aoki, and M. Matsuda. 2005. Mechanism and role of localized activation of Rho-family GTPases in growth factor-stimulated fibroblasts and neuronal cells. Biochem Soc Trans 33:631-634.

36. Ditlev, J. A., N. M. Vacanti, I. L. Novak, and L. M. Loew. 2009. An open model of actin dendritic nucleation. Biophys J 96:3529-3542.

37. Blanchoin, L., K. J. Amann, H. N. Higgs, J. B. Marchand, D. A. Kaiser, and T. D. Pollard. 2000. Direct observation of dendritic actin filament networks nucleated by Arp2/3 complex and WASP/Scar proteins. Nature 404:1007-1011.

38. Peskin, C. S., G. M. Odell, and G. F. Oster. 1993. Cellular motions and thermal fluctuations: the Brownian ratchet. Biophys J 65:316-324.

39. Fraley, T. S., T. C. Tran, A. M. Corgan, C. A. Nash, J. Hao, D. R. Critchley, and J. A. Greenwood. 2003. Phosphoinositide binding inhibits alpha-actinin bundling activity. J Biol Chem 278:24039-24045.

40. Yang, L., D. Sept, and A. E. Carlsson. 2006. Energetics and dynamics of constrained actin filament bundling. Biophys J 90:4295-4304.

41. Yu, X. and A. E. Carlsson. 2004. Kinetics of filament bundling with attractive interactions. Biophys J 87:3679-3689.

42. Svitkina, T. M. and G. G. Borisy. 1999. Arp2/3 complex and actin depolymerizing factor/cofilin in dendritic organization and treadmilling of actin filament array in lamellipodia. J Cell Biol. 145:1009-1026.

43. Urban, E., S. Jacob, M. Nemethova, G. P. Resch, and J. V. Small. 2010. Electron tomography reveals unbranched networks of actin filaments in lamellipodia. Nat Cell Biol 12:429-435.

44. Gauthier, N. C., O. M. Rossier, A. Mathur, J. C. Hone, and M. P. Sheetz. 2009. Plasma membrane area increases with spread area by exocytosis of a GPI-anchored protein compartment. Mol Biol Cell 20:3261-3272.

45. Roca-Cusachs, P., N. C. Gauthier, A. Del Rio, and M. P. Sheetz. 2009. Clustering of alpha(5)beta(1) integrins determines adhesion strength whereas alpha(v)beta(3) and talin enable mechanotransduction. Proc Natl Acad Sci U S A 106:16245-16250.

46. Sheetz, M. P., D. P. Felsenfeld, and C. G. Galbraith. 1998. Cell migration: regulation of force on extracellular-matrix-integrin complexes. Trends Cell Biol 8:51-54.

47. von Wichert, G., B. Haimovich, G. S. Feng, and M. P. Sheetz. 2003. Force-dependent integrin-cytoskeleton linkage formation requires downregulation of focal complex dynamics by Shp2. Embo J 22:5023-5035.

48. Worth, D. C., K. Hodivala-Dilke, S. D. Robinson, S. J. King, P. E. Morton, F. B. Gertler, M. J. Humphries, and M. Parsons. 2010. Alpha v beta3 integrin spatially regulates VASP and RIAM to control adhesion dynamics and migration. J Cell Biol 189:369-383.

49. Xu, C., J. Watras, and L. M. Loew. 2003. Kinetic analysis of receptor-activated phosphoinositide turnover. J Cell Biol 161:779-791.

50. Nolen, B. J., N. Tomasevic, A. Russell, D. W. Pierce, Z. Jia, C. D. McCormick, J. Hartman, R. Sakowicz, and T. D. Pollard. 2009. Characterization of two classes of small molecule inhibitors of Arp2/3 complex. Nature 460:1031-1034.

51. Tvorogov, D., X. J. Wang, R. Zent, and G. Carpenter. 2005. Integrin-dependent PLC-gamma1 phosphorylation mediates fibronectin-dependent adhesion. J Cell Sci 118:601-610.

52. Hamasaki, K., T. Mimura, N. Morino, H. Furuya, T. Nakamoto, S. Aizawa, C. Morimoto, Y. Yazaki, H. Hirai, and Y. Nojima. 1996. Src kinase plays an essential role in integrin-mediated tyrosine phosphorylation of Crk-associated substrate p130Cas. Biochem Biophys Res Commun 222:338-343.

53. Vuori, K., H. Hirai, S. Aizawa, and E. Ruoslahti. 1996. Introduction of p130cas signaling complex formation upon integrin-mediated cell adhesion: a role for Src family kinases. Mol Cell Biol 16:2606-2613.

54. Takagi, J., K. Strokovich, T. A. Springer, and T. Walz. 2003. Structure of integrin alpha5beta1 in complex with fibronectin. Embo J 22:4607-4615.

55. Withers, B. E., P. R. Keller, and D. W. Fry. 1996. Expression, purification and characterization of focal adhesion kinase using a baculovirus system. Protein Expr Purif 7:12-18.

56. Mitra, S. K., D. A. Hanson, and D. D. Schlaepfer. 2005. Focal adhesion kinase: in command and control of cell motility. Nat Rev Mol Cell Biol 6:56-68.

57. Sugimoto, S., R. J. Lechleider, S. E. Shoelson, B. G. Neel, and C. T. Walsh. 1993. Expression, purification, and characterization of SH2-containing protein tyrosine phosphatase, SH-PTP2. J Biol Chem 268:22771-22776.

58. Burridge, K., S. K. Sastry, and J. L. Sallee. 2006. Regulation of cell adhesion by protein-tyrosine phosphatases. I. Cell-matrix adhesion. J Biol Chem 281:15593-15596.

59. Lieser, S. A., J. Shaffer, and J. A. Adams. 2006. SRC tail phosphorylation is limited by structural changes in the regulatory tyrosine kinase Csk. J Biol Chem 281:38004-38012.

60. Torres, E. and M. K. Rosen. 2006. Protein-tyrosine kinase and GTPase signals cooperate to phosphorylate and activate Wiskott-Aldrich syndrome protein (WASP)/neuronal WASP. J Biol Chem 281:3513-3520.

61. von Wichert, G., G. Jiang, A. Kostic, K. De Vos, J. Sap, and M. P. Sheetz. 2003. RPTP-alpha acts as a transducer of mechanical force on alphav/beta3-integrin-cytoskeleton linkages. J Cell Biol 161:143-153.

62. de Pereda, J. M., K. L. Wegener, E. Santelli, N. Bate, M. H. Ginsberg, D. R. Critchley, I. D. Campbell, and R. C. Liddington. 2005. Structural basis for phosphatidylinositol phosphate kinase type Igamma binding to talin at focal adhesions. J Biol Chem 280:8381-8386.

63. Calderwood, D. A., B. Yan, J. M. de Pereda, B. G. Alvarez, Y. Fujioka, R. C. Liddington, and M. H. Ginsberg. 2002. The phosphotyrosine binding-like domain of talin activates integrins. J Biol Chem 277:21749-21758.

64. Ratnikov, B. I., A. W. Partridge, and M. H. Ginsberg. 2005. Integrin activation by talin. J Thromb Haemost 3:1783-1790.

65. Feder, D. and J. M. Bishop. 1990. Purification and enzymatic characterization of pp60c-src from human platelets. J Biol Chem 265:8205-8211.

66. Niu, T., X. Liang, J. Yang, Z. Zhao, and G. W. Zhou. 1999. Kinetic comparison of the catalytic domains of SHP-1 and SHP-2. J Cell Biochem 72:145-150.

67. Ishihara, H., Y. Shibasaki, N. Kizuki, T. Wada, Y. Yazaki, T. Asano, and Y. Oka. 1998. Type I phosphatidylinositol-4-phosphate 5-kinases. Cloning of the third isoform and deletion/substitution analysis of members of this novel lipid kinase family. J Biol Chem 273:8741-8748.

68. McConnachie, G., I. Pass, S. M. Walker, and C. P. Downes. 2003. Interfacial kinetic analysis of the tumour suppressor phosphatase, PTEN: evidence for activation by anionic phospholipids. Biochem J 371:947-955.

69. Matzaris, M., S. P. Jackson, K. M. Laxminarayan, C. J. Speed, and C. A. Mitchell. 1994. Identification and characterization of the phosphatidylinositol-(4, 5)-bisphosphate 5-phosphatase in human platelets. J Biol Chem 269:3397-3402.

70. Raftopoulou, M. and A. Hall. 2004. Cell migration: Rho GTPases lead the way. Dev Biol 265:23-32.

71. Meier, T. I., J. A. Cook, J. E. Thomas, J. A. Radding, C. Horn, T. Lingaraj, and M. C. Smith. 2004. Cloning, expression, purification, and characterization of the human Class Ia phosphoinositide 3-kinase isoforms. Protein Expr Purif 35:218-224.

72. Zhai, J., H. Lin, Z. Nie, J. Wu, R. Canete-Soler, W. W. Schlaepfer, and D. D. Schlaepfer. 2003. Direct interaction of focal adhesion kinase with p190RhoGEF. J Biol Chem 278:24865-24873.

73. Wells, C. D., S. Gutowski, G. Bollag, and P. C. Sternweis. 2001. Identification of potential mechanisms for regulation of p115 RhoGEF through analysis of endogenous and mutant forms of the exchange factor. J Biol Chem 276:28897-28905.

74. Zhang, B. and Y. Zheng. 1998. Regulation of RhoA GTP hydrolysis by the GTPase-activating proteins p190, p50RhoGAP, Bcr, and 3BP-1. Biochemistry 37:5249-5257.

75. Hall, A. 2005. Rho GTPases and the control of cell behaviour. Biochem Soc Trans 33:891-895.

76. Zhang, B., J. Chernoff, and Y. Zheng. 1998. Interaction of Rac1 with GTPase-activating proteins and putative effectors. A comparison with Cdc42 and RhoA. J Biol Chem 273:8776-8782.

77. Santarius, M., C. H. Lee, and R. A. Anderson. 2006. Supervised membrane swimming: small G-protein lifeguards regulate PIPK signalling and monitor intracellular PtdIns(4,5)P2 pools. Biochem J 398:1-13.

78. Blumenstein, L. and M. R. Ahmadian. 2004. Models of the cooperative mechanism for Rho effector recognition: implications for RhoA-mediated effector activation. J Biol Chem 279:53419-53426.

79. Doran, J. D., X. Liu, P. Taslimi, A. Saadat, and T. Fox. 2004. New insights into the structure-function relationships of Rho-associated kinase: a thermodynamic and hydrodynamic study of the dimer-to-monomer transition and its kinetic implications. Biochem J 384:255-262.

80. Prasad, N., R. S. Topping, and S. J. Decker. 2001. SH2-containing inositol 5'-phosphatase SHIP2 associates with the p130(Cas) adapter protein and regulates cellular adhesion and spreading. Mol Cell Biol 21:1416-1428.

81. Parker, K. K., A. L. Brock, C. Brangwynne, R. J. Mannix, N. Wang, E. Ostuni, N. A. Geisse, J. C. Adams, G. M. Whitesides, and D. E. Ingber. 2002. Directional control of

lamellipodia extension by constraining cell shape and orienting cell tractional forces. Faseb J 16:1195-1204.

82. Zhang, B., Z. X. Wang, and Y. Zheng. 1997. Characterization of the interactions between the small GTPase Cdc42 and its GTPase-activating proteins and putative effectors. Comparison of kinetic properties of Cdc42 binding to the Cdc42-interactive domains. J Biol Chem 272:21999-22007.

83. Hemsath, L. and M. R. Ahmadian. 2005. Fluorescence approaches for monitoring interactions of Rho GTPases with nucleotides, regulators, and effectors. Methods 37:173-182.

84. Weaver, A. M., M. E. Young, W. L. Lee, and J. A. Cooper. 2003. Integration of signals to the Arp2/3 complex. Curr Opin Cell Biol 15:23-30.

85. Marchand, J. B., D. A. Kaiser, T. D. Pollard, and H. N. Higgs. 2001. Interaction of WASP/Scar proteins with actin and vertebrate Arp2/3 complex. Nat Cell Biol 3:76-82.

86. Higgs, H. N. and T. D. Pollard. 2000. Activation by Cdc42 and PIP(2) of Wiskott-Aldrich syndrome protein (WASp) stimulates actin nucleation by Arp2/3 complex. J Cell Biol 150:1311-1320.

87. Ten Klooster, J. P., E. E. Evers, L. Janssen, L. M. Machesky, F. Michiels, P. Hordijk, and J. G. Collard. 2006. Interaction between Tiam1 and the Arp2/3 complex links activation of Rac to actin polymerization. Biochem J 397:39-45.

88. Niggli, V. 2005. Regulation of protein activities by phosphoinositide phosphates. Annu Rev Cell Dev Biol 21:57-79.

89. Xian, W. and P. A. Janmey. 2002. Dissecting the gelsolin-polyphosphoinositide interaction and engineering of a polyphosphoinositide-sensitive gelsolin C-terminal half protein. J Mol Biol 322:755-771.

90. Janmey, P. A., J. Lamb, P. G. Allen, and P. T. Matsudaira. 1992. Phosphoinositide-binding peptides derived from the sequences of gelsolin and villin. J Biol Chem 267:11818-11823.

91. Schafer, D. A., P. B. Jennings, and J. A. Cooper. 1996. Dynamics of capping protein and actin assembly in vitro: uncapping barbed ends by polyphosphoinositides. J Cell Biol 135:169-179.

92. Eungdamrong, N. J. and R. Iyengar. 2007. Compartment-specific feedback loop and regulated trafficking can result in sustained activation of Ras at the Golgi. Biophys J 92:808-815.

93. Ono, S. 2007. Mechanism of depolymerization and severing of actin filaments and its significance in cytoskeletal dynamics. Int Rev Cytol 258:1-82.

94. Hernjak, N., B. M. Slepchenko, K. Fernald, C. C. Fink, D. Fortin, Moraru, II, J. Watras, and L. M. Loew. 2005. Modeling and analysis of calcium signaling events leading to long-term depression in cerebellar Purkinje cells. Biophys J 89:3790-3806.

95. Singh, S. S., A. Chauhan, N. Murakami, and V. P. Chauhan. 1996. Profilin and gelsolin stimulate phosphatidylinositol 3-kinase activity. Biochemistry 35:16544-16549.

96. Otey, C. A., F. M. Pavalko, and K. Burridge. 1990. An interaction between alpha-actinin and the beta 1 integrin subunit in vitro. J Cell Biol 111:721-729.

97. Crawford, A. W., J. W. Michelsen, and M. C. Beckerle. 1992. An interaction between zyxin and alpha-actinin. J Cell Biol 116:1381-1393.

98. Ball, L. J., R. Kuhne, B. Hoffmann, A. Hafner, P. Schmieder, R. Volkmer-Engert, M. Hof, M. Wahl, J. Schneider-Mergener, U. Walter, H. Oschkinat, and T. Jarchau. 2000. Dual epitope recognition by the VASP EVH1 domain modulates polyproline ligand specificity and binding affinity. Embo J 19:4903-4914.

99. Kang, F., R. O. Laine, M. R. Bubb, F. S. Southwick, and D. L. Purich. 1997. Profilin interacts with the Gly-Pro-Pro-Pro-Pro-Pro sequences of vasodilator-stimulated phosphoprotein (VASP): implications for actin-based Listeria motility. Biochemistry 36:8384-8392.

100. Goldschmidt-Clermont, P. J., L. M. Machesky, J. J. Baldassare, and T. D. Pollard. 1990. The actin-binding protein profilin binds to PIP2 and inhibits its hydrolysis by phospholipase C. Science 247:1575-1578.

101. Pollard, T. D., L. Blanchoin, and R. D. Mullins. 2000. Molecular mechanisms controlling actin filament dynamics in nonmuscle cells. Annu Rev Biophys Biomol Struct 29:545-576.

102. Michaelson, D., J. Silletti, G. Murphy, P. D'Eustachio, M. Rush, and M. R. Philips. 2001. Differential localization of Rho GTPases in live cells: regulation by hypervariable regions and RhoGDI binding. J Cell Biol 152:111-126.

103. Ellis, R. J. 2001. Macromolecular crowding: obvious but underappreciated. Trends Biochem Sci 26:597-604.

104. Delibrias, C. C., J. E. Floettmann, M. Rowe, and D. T. Fearon. 1997. Downregulated expression of SHP-1 in Burkitt lymphomas and germinal center B lymphocytes. J Exp Med 186:1575-1583.

105. Higgs, H. N., L. Blanchoin, and T. D. Pollard. 1999. Influence of the C terminus of Wiskott-Aldrich syndrome protein (WASp) and the Arp2/3 complex on actin polymerization. Biochemistry 38:15212-15222.

106. Dubin-Thaler, B. J., G. Giannone, H. G. Dobereiner, and M. P. Sheetz. 2004. Nanometer analysis of cell spreading on matrix-coated surfaces reveals two distinct cell states and STEPs. Biophys J 86:1794-1806.

107. Faeder, J. R., W. S. Hlavacek, I. Reischl, M. L. Blinov, H. Metzger, A. Redondo, C. Wofsy, and B. Goldstein. 2003. Investigation of early events in Fc epsilon RI-mediated signaling using a detailed mathematical model. J Immunol 170:3769-3781.

108. Wiseman, P. W., C. M. Brown, D. J. Webb, B. Hebert, N. L. Johnson, J. A. Squier, M. H. Ellisman, and A. F. Horwitz. 2004. Spatial mapping of integrin interactions and dynamics during cell migration by image correlation microscopy. J Cell Sci 117:5521-5534.

109. Bear, J. E., T. M. Svitkina, M. Krause, D. A. Schafer, J. J. Loureiro, G. A. Strasser, I. V. Maly, O. Y. Chaga, J. A. Cooper, G. G. Borisy, and F. B. Gertler. 2002. Antagonism between Ena/VASP proteins and actin filament capping regulates fibroblast motility. Cell 109:509-521.

110. Pollard, T. D., L. Blanchoin, and M. R. D. 2000. Molecular mechanisms controlling actin filament dynamics in nonmuscle cells. Annu Rev. Biophys. Biomol. Struct. 29:545-576.

111. Howard, J. 2001. Mechanics of motor proteins and the cytoskeleton. Sunderland MA: Sinauer Associates Inc.

112. Robinson, R. C., K. Turbedsky, D. A. Kaiser, J. B. Marchand, H. N. Higgs, S. Choe, and T. D. Pollard. 2001. Crystal structure of Arp2/3 complex. Science 294:1679-1684.

113. Medalia, O., I. Weber, A. S. Frangakis, D. Nicastro, G. Gerisch, and W. Baumeister. 2002. Macromolecular architecture in eukaryotic cells visualized by cryoelectron tomography. Science 298:1209-1213.

114. Higgs, H. N. and T. D. Pollard. 2001. Regulation of actin filament network formation through ARP2/3 complex: activation by a diverse array of proteins. Annu Rev Biochem 70:649-676.

115. Volkmann, N., K. J. Amann, S. Stoilova-McPhie, C. Egile, D. C. Winter, L. Hazelwood, J. E. Heuser, R. Li, T. D. Pollard, and D. Hanein. 2001. Structure of Arp2/3 complex in its activated state and in actin filament branch junctions. Science 293:2456-2459.

116. Raucher, D. and M. P. Sheetz. 1999. Characteristics of a membrane reservoir buffering membrane tension. Biophys J 77:1992-2002.

117. Abraham, V. C., V. Krishnamurthi, D. L. Taylor, and F. Lanni. 1999. The actin-based nanomachine at the leading edge of migrating cells. Biophys J 77:1721-1732.

118. Pollard, T. D. and G. G. Borisy. 2003. Cellular motility driven by assembly and disassembly of actin filaments. Cell 112:453-465.

Figure S1

Module 1: Early events

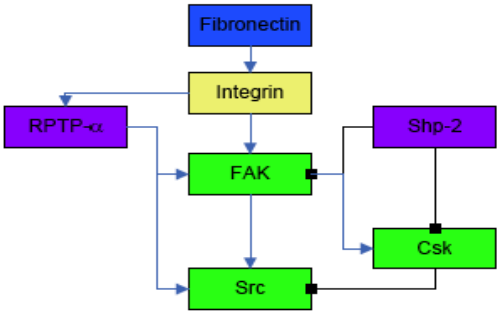

Module 2: Talin, PIPKI activation

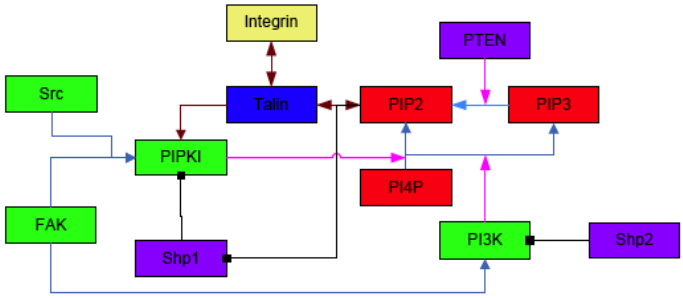

Module 3: Rho activation

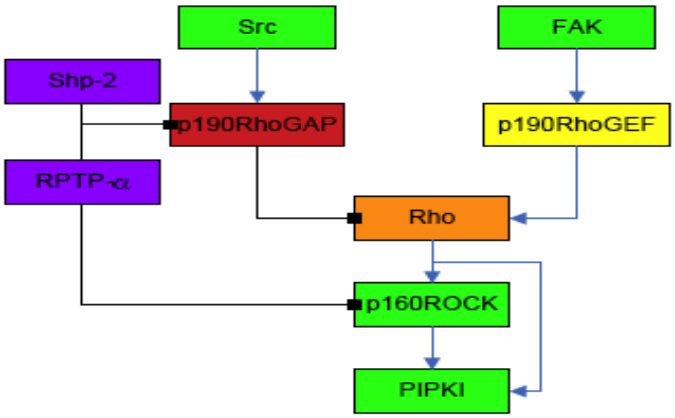

Module 4: Rac activation

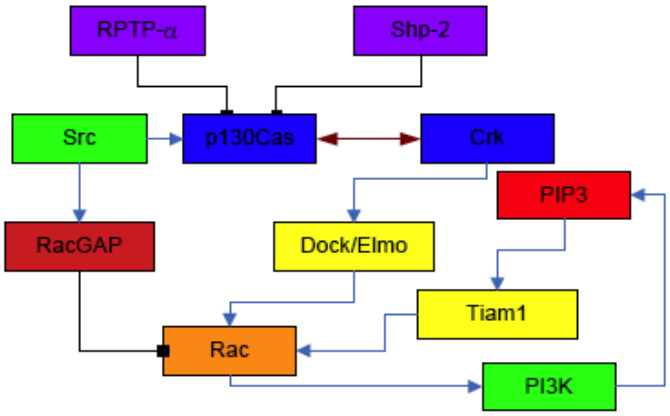

Module 5: Cdc42 activation

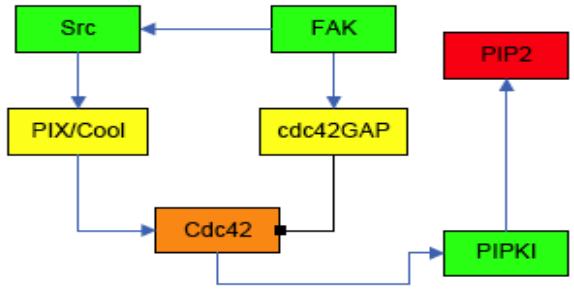

Module 6: Arp2/3 activation

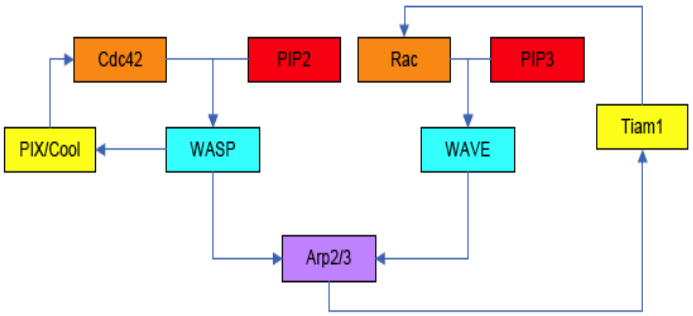

Module 7: Profilin activation

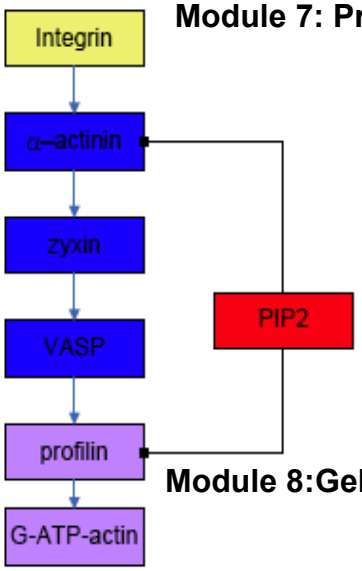

Module 8:Gelsolin activation

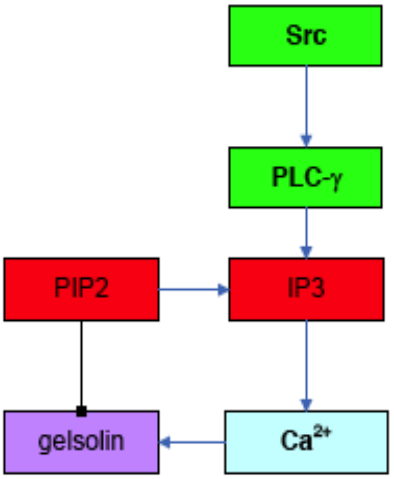

Figure S2

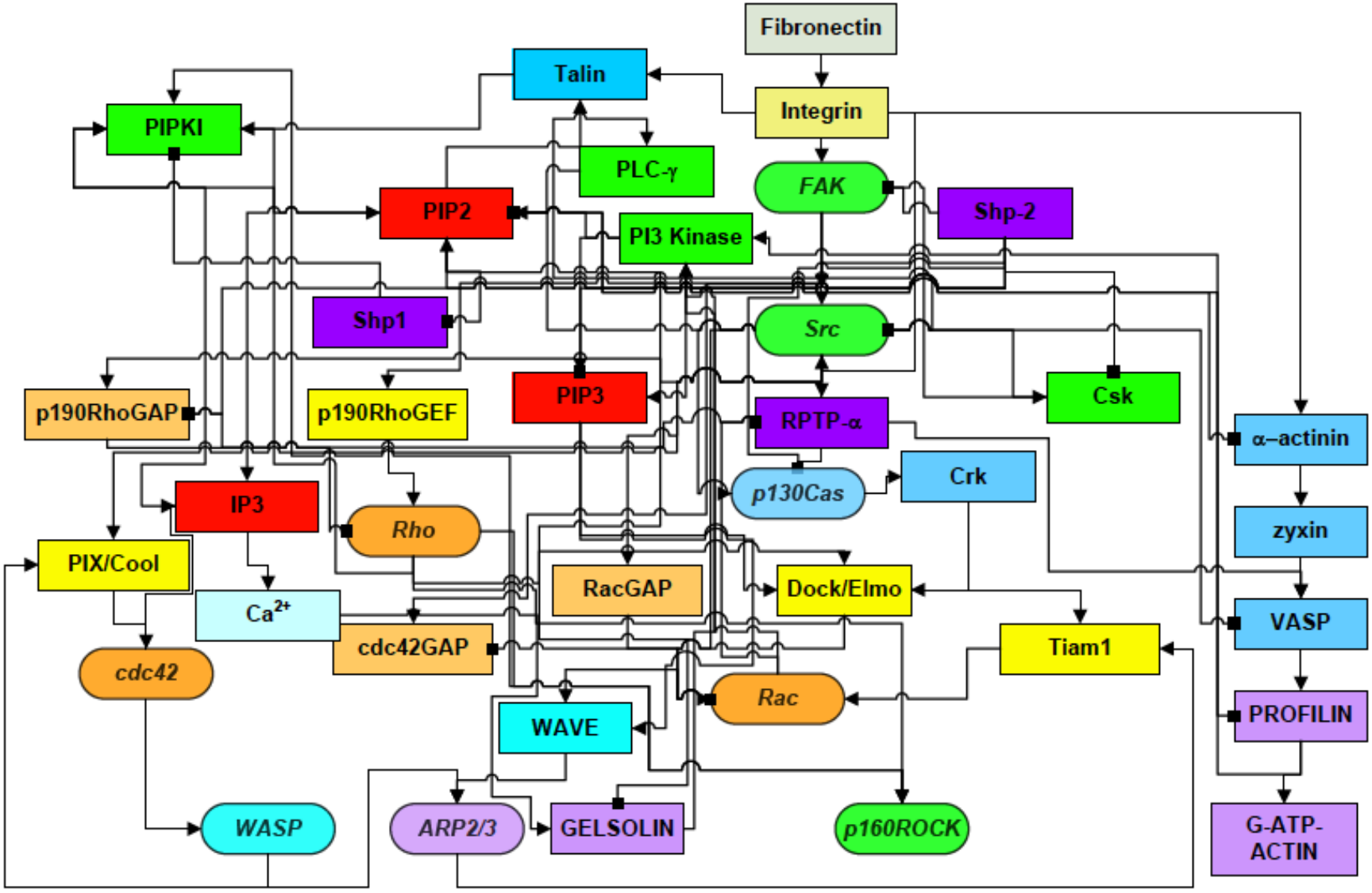
Fibronectin
Talin
Integrin
PIPKI
PLC-γ
FAK
Shp-2
PIP2
PI3 Kinase
Shp1
Src
Csk
p190RhoGAP
p190RhoGEF
PIP3
RPTP-α
α–actinin
Crk
p130Cas
IP3
Rho
zyxin
PIX/Cool
RacGAP
Dock/Elmo
Ca2+
cdc42GAP
VASP
Tiam1
cdc42
Rac
PROFILIN
WAVE
WASP
ARP2/3
GELSOLIN
p160ROCK
G-ATP-ACTIN

Figure S3

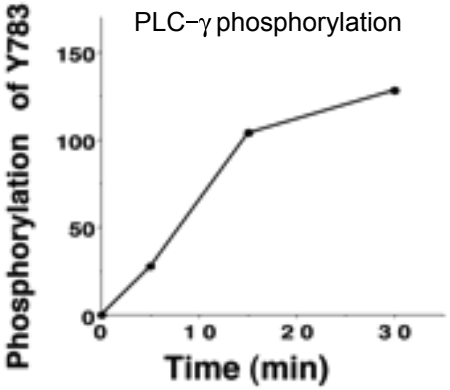

Obtain image file from literature reference

Obtain time-course data from simulations

Time (min)	Concentration from Simulation
0	0
5	0.11
15	0.27
30	0.33

Time (min)	ImageJ measurement (arbitrary units)
0	0
5	19
15	69
30	84

Use ImageJ measurement tools to convert image file data into tabular form

Normalize simulation data using maximum concentration

Time (min)	Concentration from Simulation	Normalized Concentration
0	0	0
5	0.11	0.34
15	0.27	0.81
30	0.33	1.00

Time (min)	ImageJ measurement (arbitrary units)	Normalized Concentration
0	0	0
5	19	0.23
15	69	0.82
30	84	1.00

Normalize tabular data using maximum concentration

Compare experiments from literature with simulations

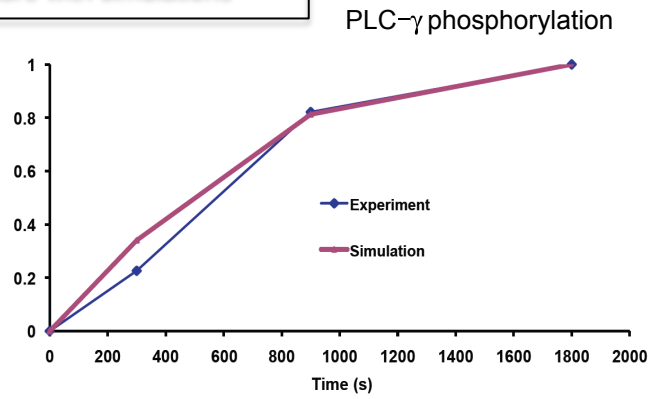

Figure S4

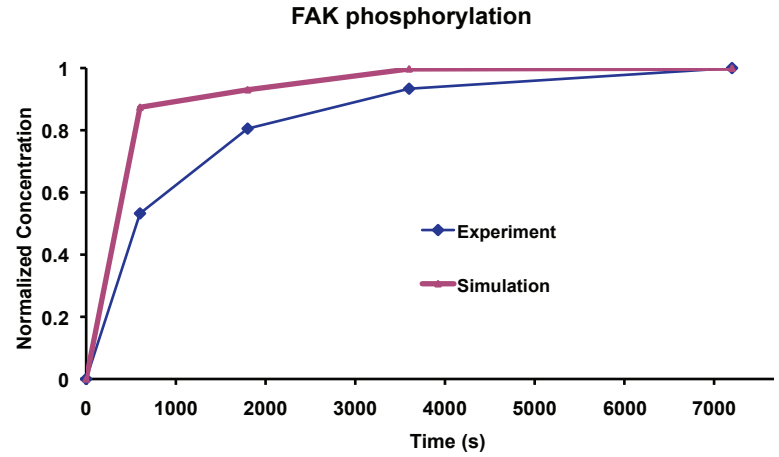
FAK phosphorylation
Normalized Concentration
Time (s)
Experiment
Simulation

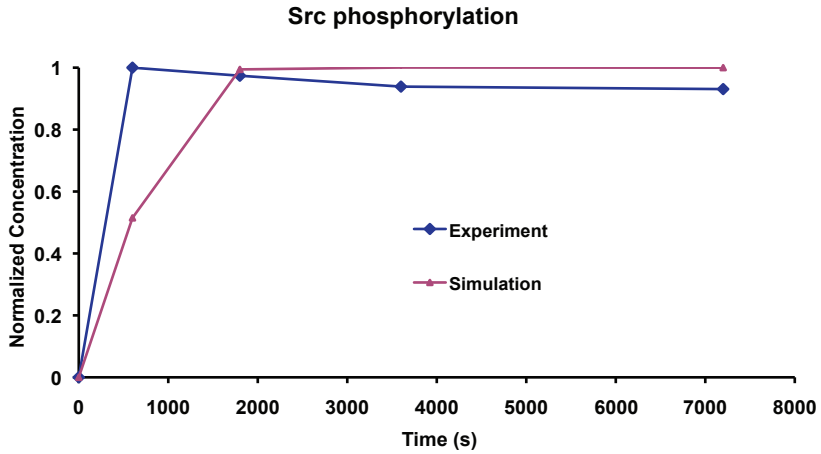
Src phosphorylation
Normalized Concentration
Time (s)
Experiment
Simulation

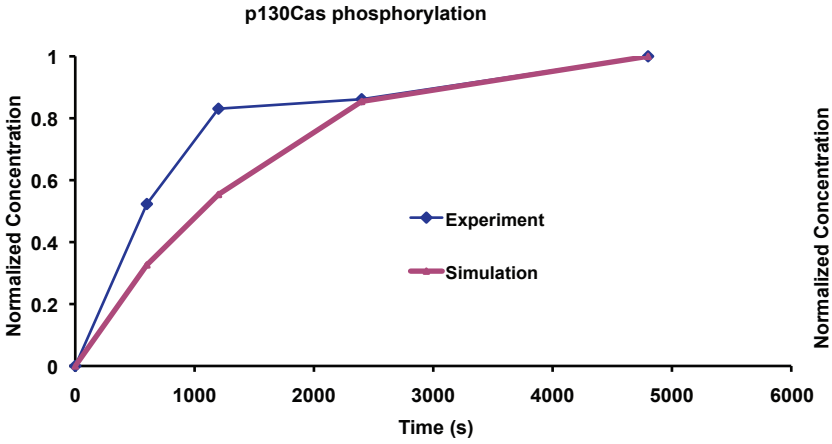
p130Cas phosphorylation
Normalized Concentration
Time (s)
Experiment
Simulation

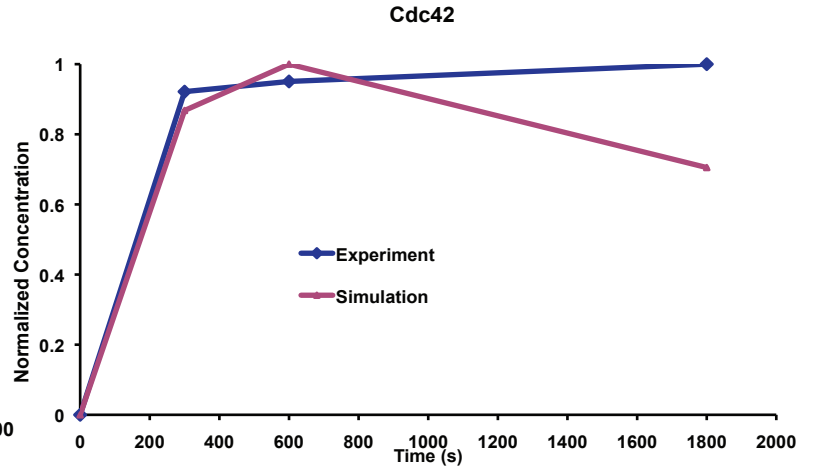
Cdc42
Normalized Concentration
Time (s)
Experiment
Simulation

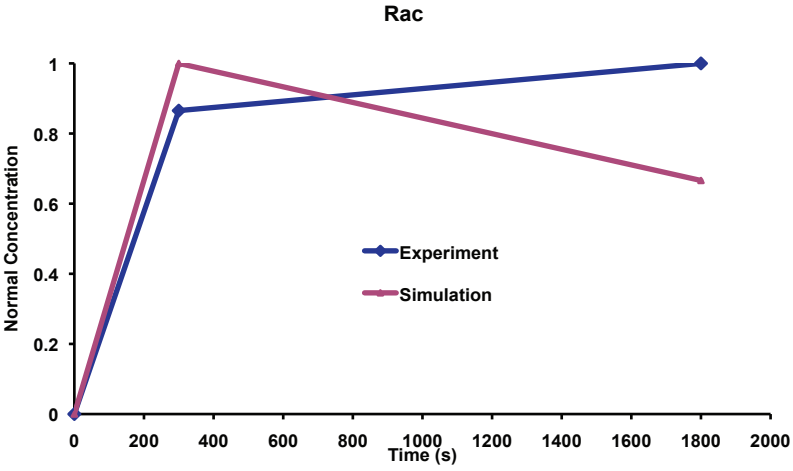
Rac
Normal Concentration
Time (s)
Experiment
Simulation

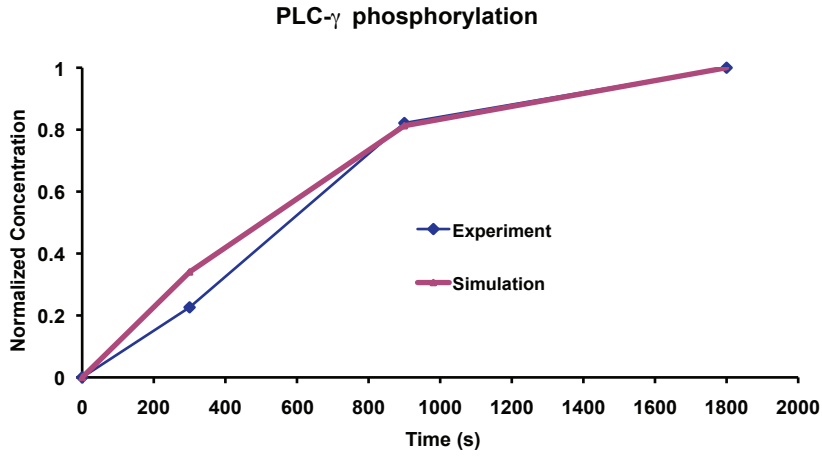
PLC-γ phosphorylation
Normalized Concentration
Time (s)
Experiment
Simulation

Figure S5

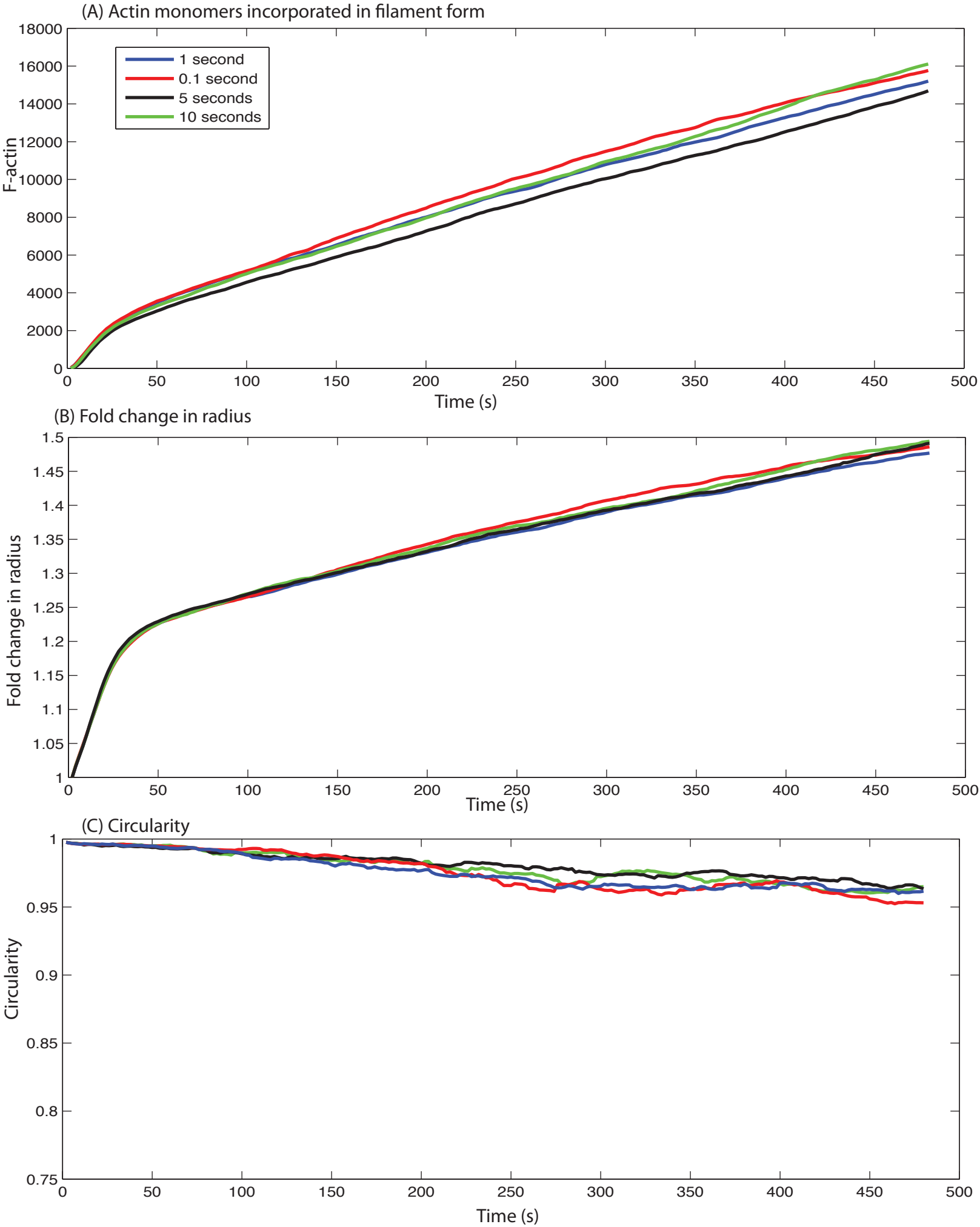
(A) Actin monomers incorporated in filament form
1 second
0.1 second
5 seconds
10 seconds
F-actin
Time (s)
(B) Fold change in radius
Fold change in radius
Time (s)
(C) Circularity
Circularity
Time (s)

Figure S6

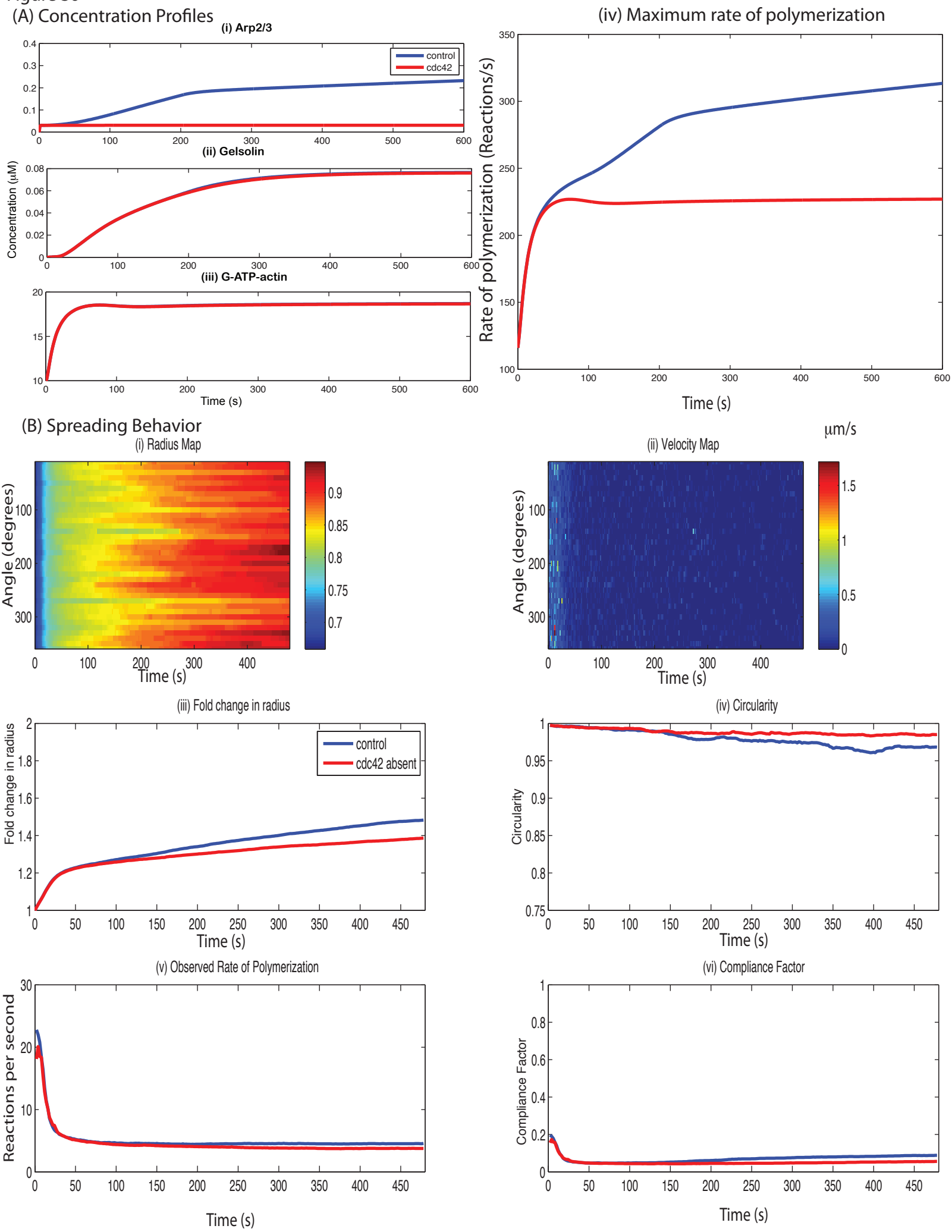
(A) Concentration Profiles
(i) Arp2/3
control
cdc42
(ii) Gelsolin
Concentration (μM)
(iii) G-ATP-actin
Time (s)
(iv) Maximum rate of polymerization
Rate of polymerization (Reactions/s)
Time (s)
(B) Spreading Behavior
(i) Radius Map
Angle (degrees)
Time (s)
μm/s
(ii) Velocity Map
Angle (degrees)
Time (s)
(iii) Fold change in radius
control
cdc42 absent
Fold change in radius
Time (s)
(iv) Circularity
Circularity
Time (s)
(v) Observed Rate of Polymerization
Reactions per second
Time (s)
(vi) Compliance Factor
Compliance Factor
Time (s)

Figure S7

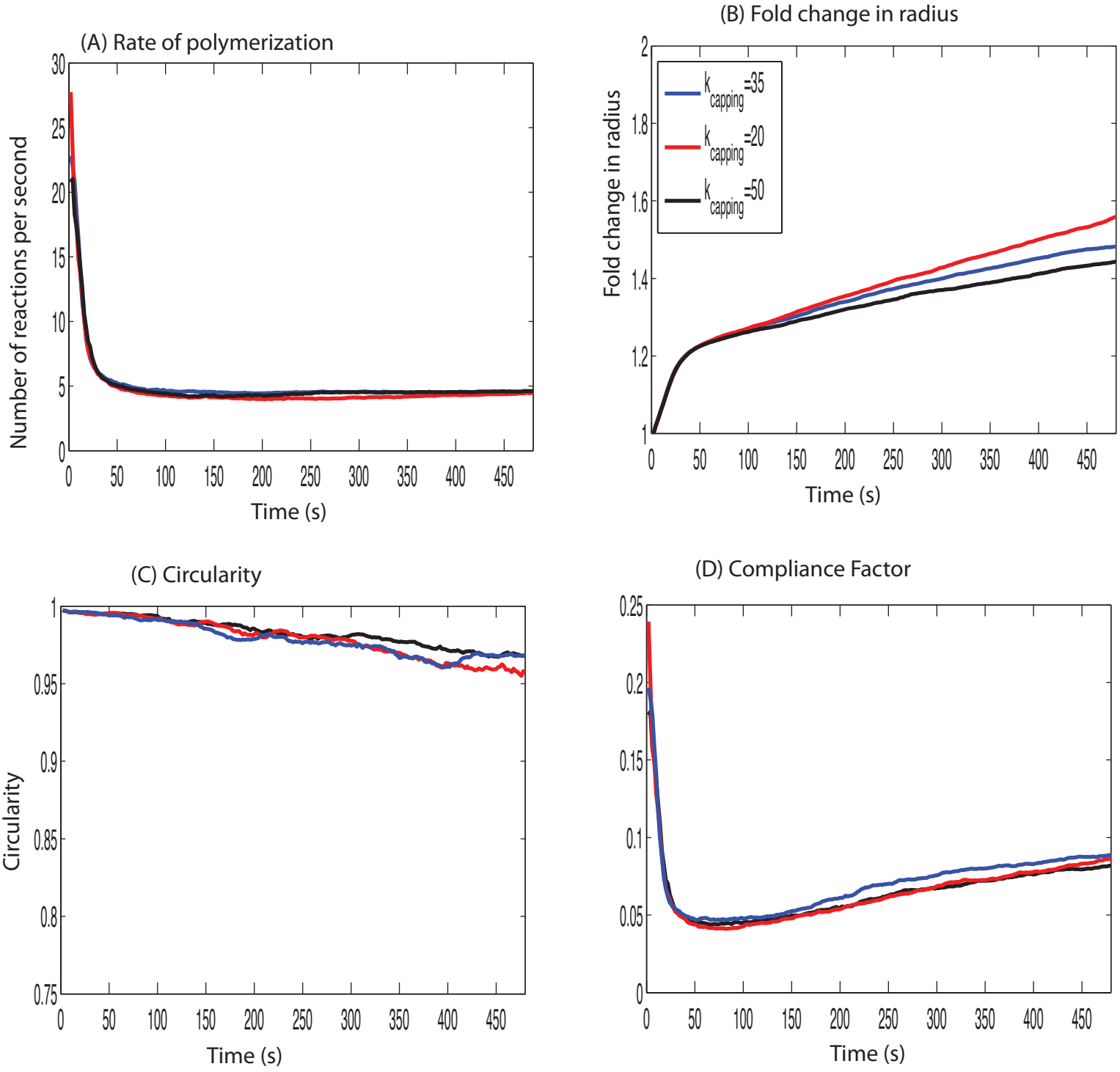
(A) Rate of polymerization
Number of reactions per second
Time (s)
(B) Fold change in radius
Fold change in radius
k capping =35
k capping =20
k capping =50
Time (s)
(C) Circularity
Circularity
Time (s)
(D) Compliance Factor
Time (s)

Figure S8

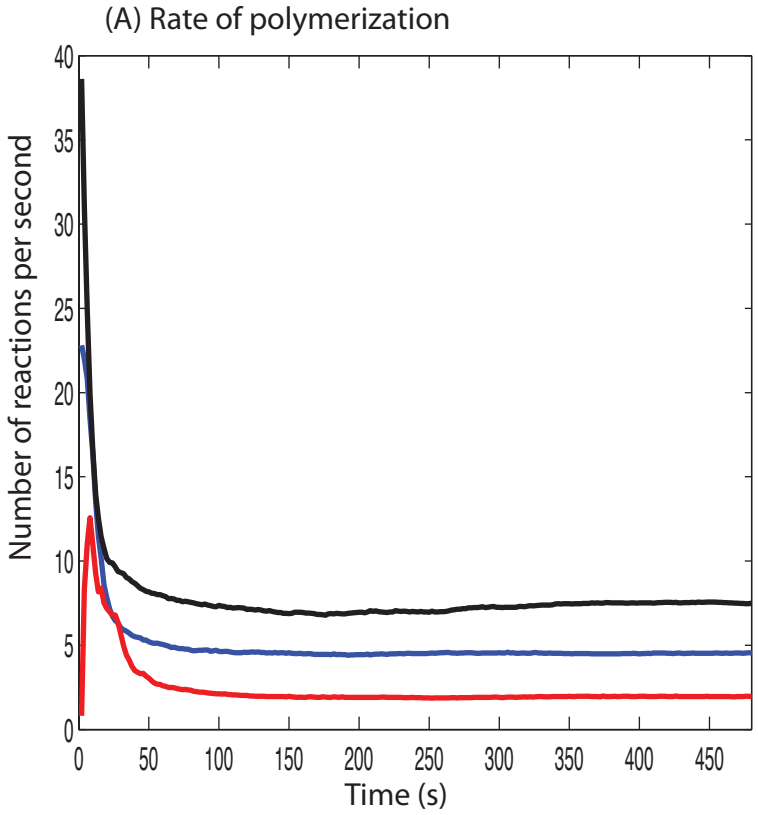
(A) Rate of polymerization
Number of reactions per second
Time (s)

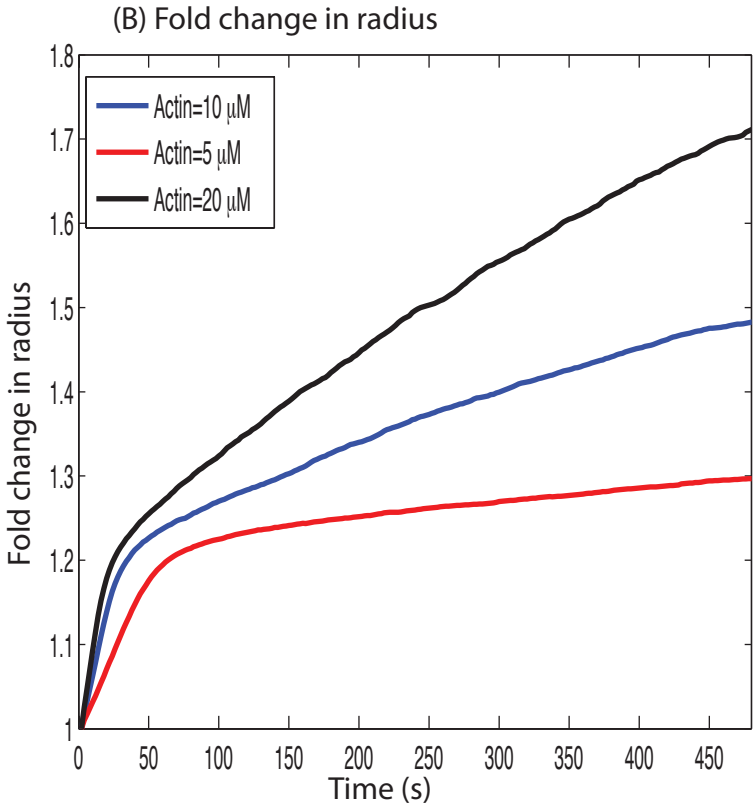
(B) Fold change in radius
Actin=10 μM
Actin=5 μM
Actin=20 μM
Fold change in radius
Time (s)

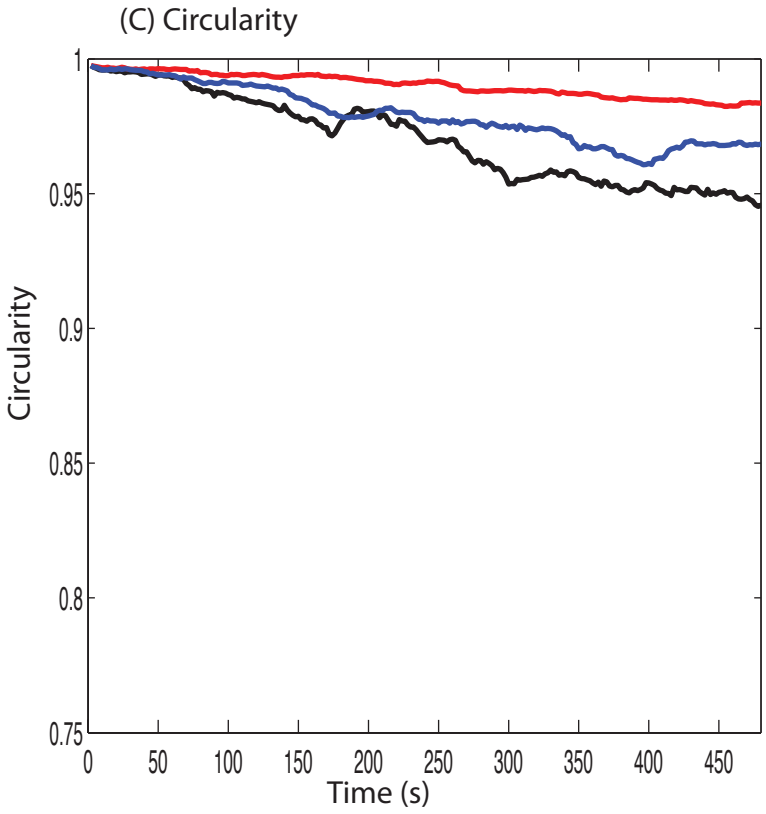
(C) Circularity
Circularity
Time (s)

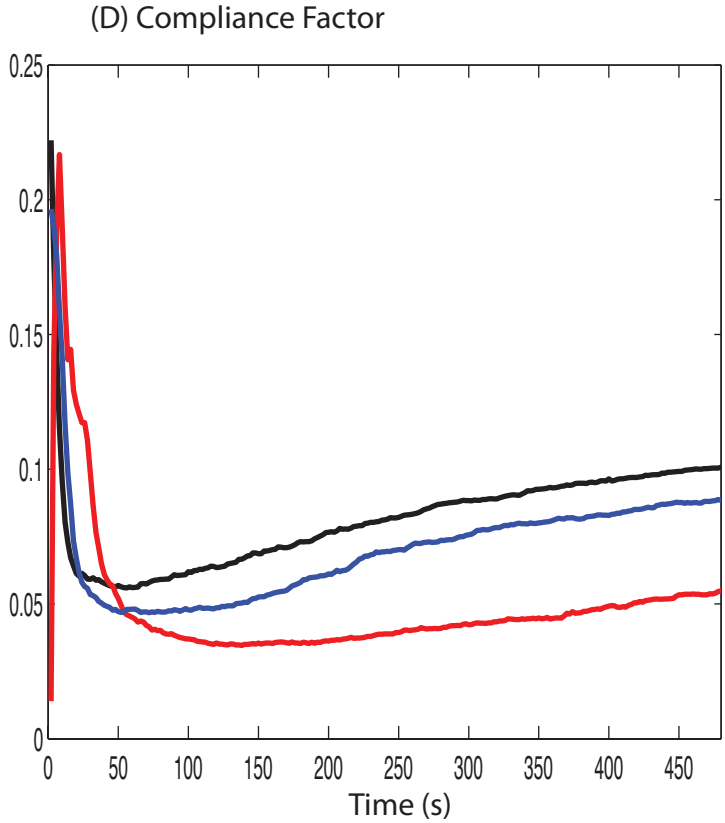
(D) Compliance Factor
Time (s)

Figure S9

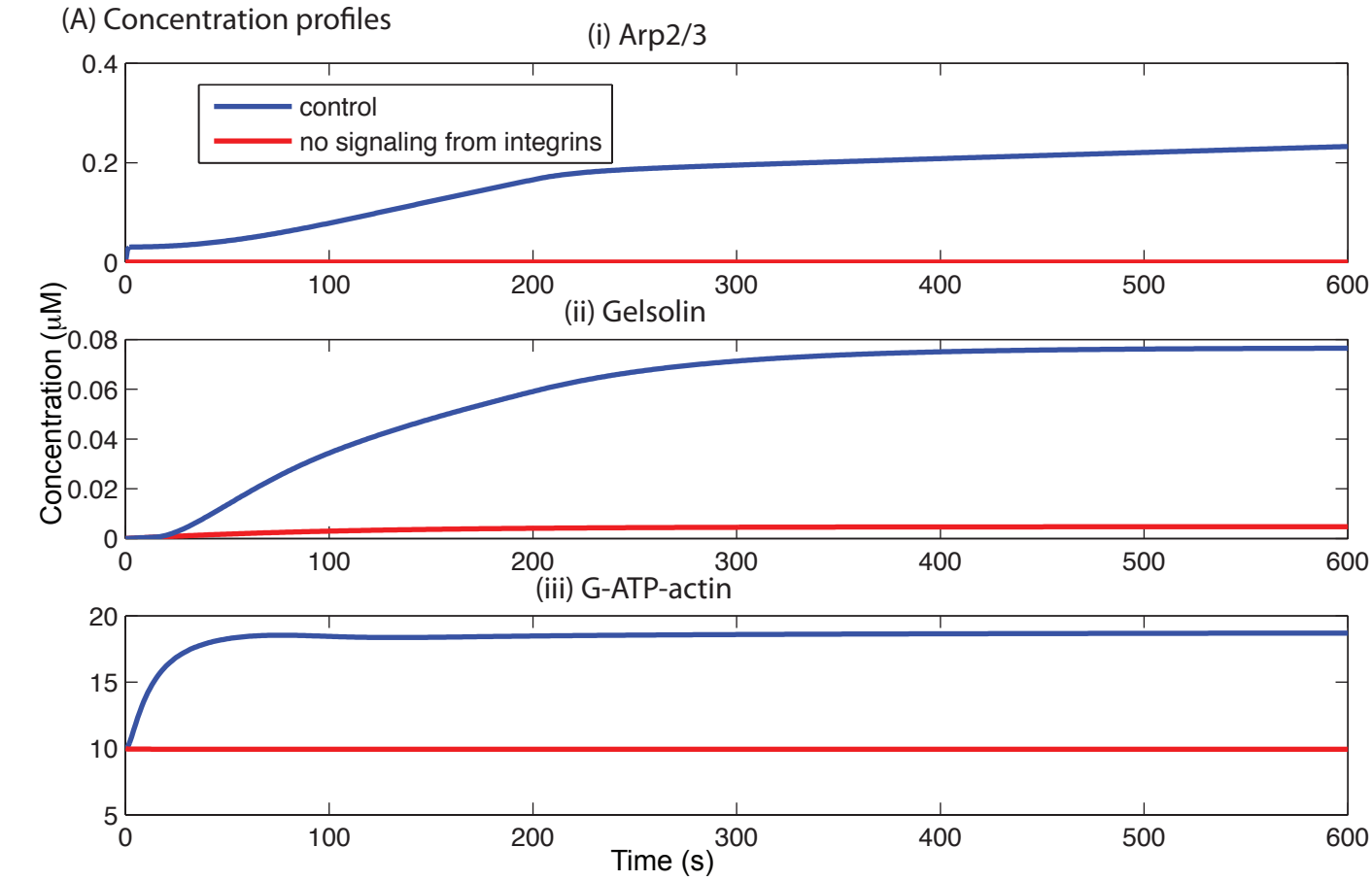
(A) Concentration profiles
(i) Arp2/3
control
no signaling from integrins
(ii) Gelsolin
(iii) G-ATP-actin
Concentration (μM)
Time (s)

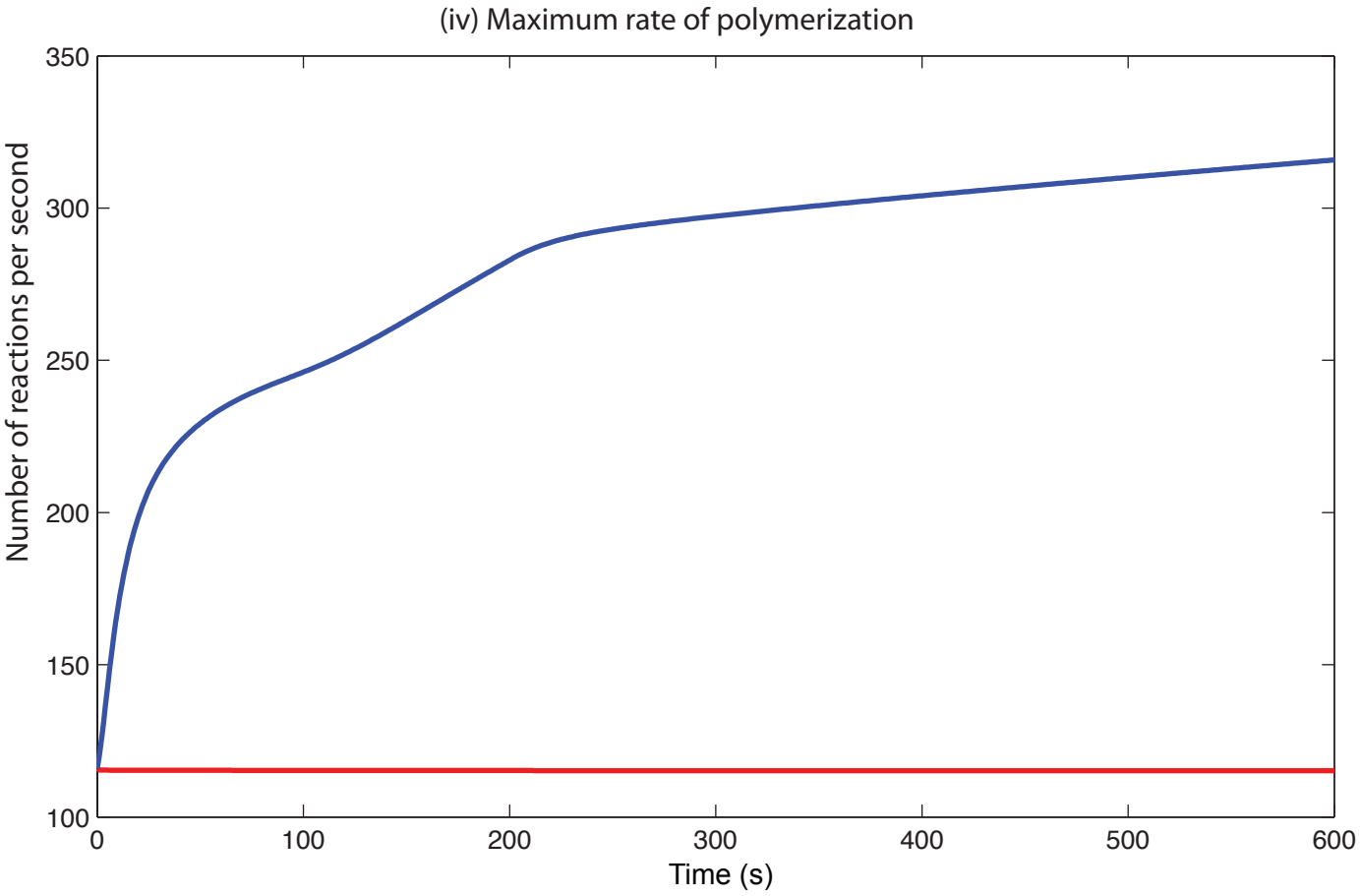
(iv) Maximum rate of polymerization
Number of reactions per second
Time (s)

Figure S10

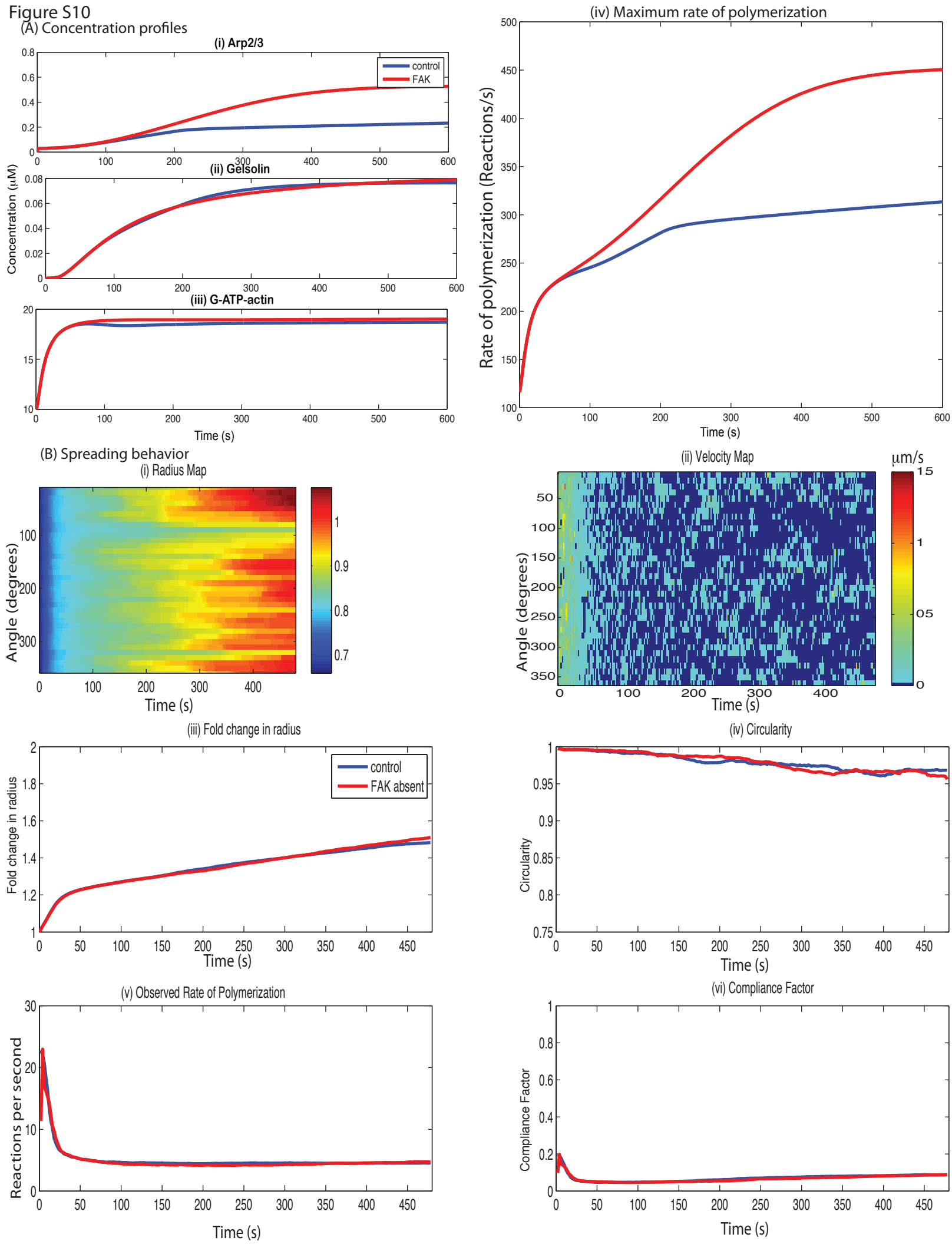
(A) Concentration profiles
(i) Arp2/3
control
FAK
(ii) Gelsolin
(iii) G-ATP-actin
Concentration (μM)
Time (s)
(iv) Maximum rate of polymerization
Rate of polymerization (Reactions/s)
Time (s)
(B) Spreading behavior
(i) Radius Map
Angle (degrees)
Time (s)
(ii) Velocity Map
μm/s
Angle (degrees)
Time (s)
(iii) Fold change in radius
control
FAK absent
Fold change in radius
Time (s)
(iv) Circularity
Circularity
Time (s)
(v) Observed Rate of Polymerization
Reactions per second
Time (s)
(vi) Compliance Factor
Compliance Factor
Time (s)

Figure S11

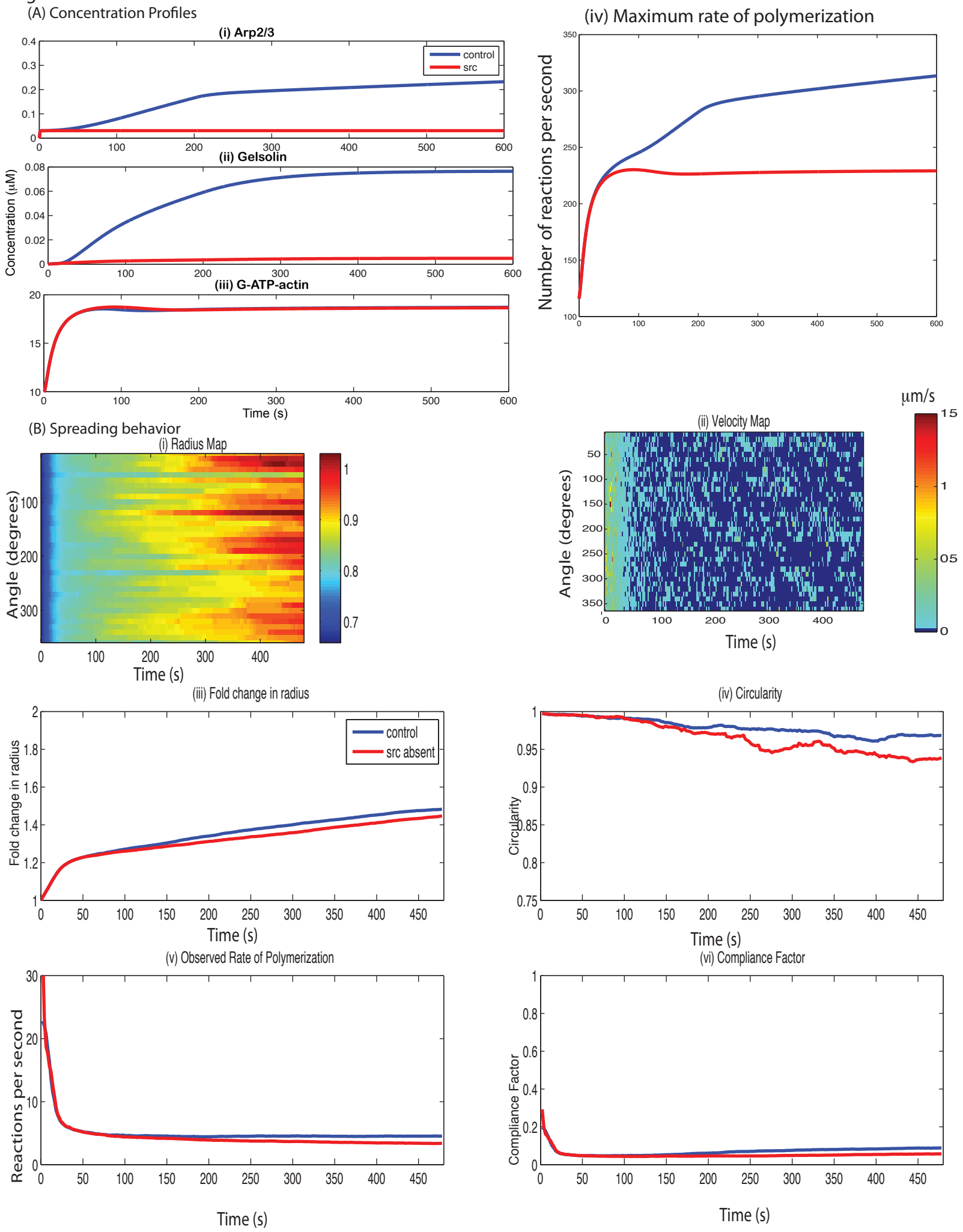
(A) Concentration Profiles
(i) Arp2/3
control
src
(ii) Gelsolin
Concentration (μM)
(iii) G-ATP-actin
Time (s)
(iv) Maximum rate of polymerization
Number of reactions per second
(B) Spreading behavior
(i) Radius Map
Angle (degrees)
Time (s)
(ii) Velocity Map
μm/s
(iii) Fold change in radius
Fold change in radius
control
src absent
Time (s)
(iv) Circularity
Circularity
Time (s)
(v) Observed Rate of Polymerization
Reactions per second
Time (s)
(vi) Compliance Factor
Compliance Factor
Time (s)

Figure S12

(A) Concentration Profiles

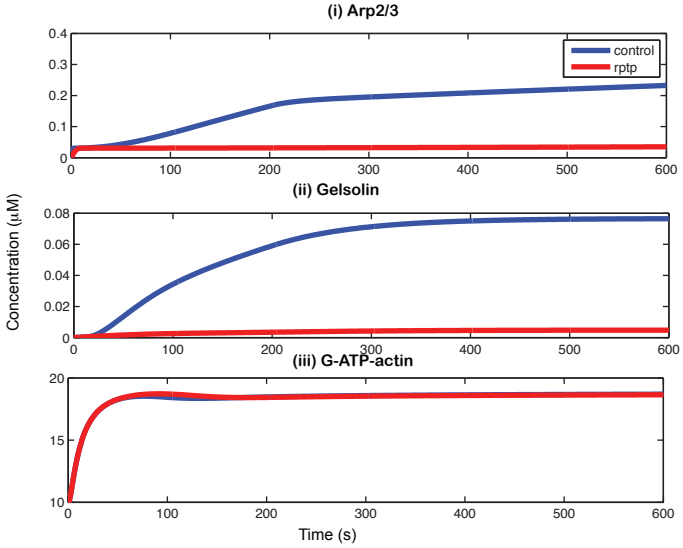

(iv) Maximum rate of polymerization

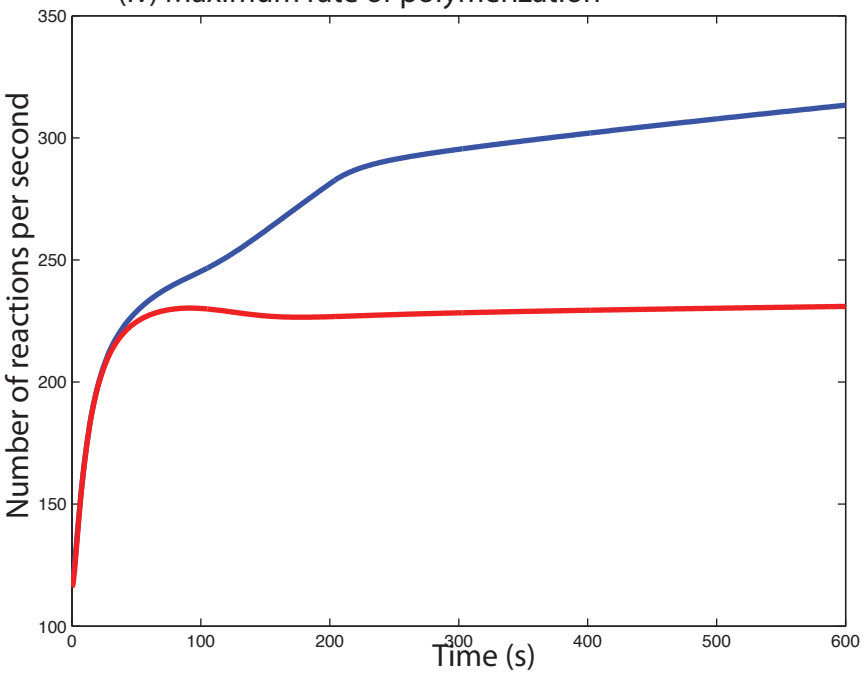

(B) Spreading Behavior

(i) Radius Map

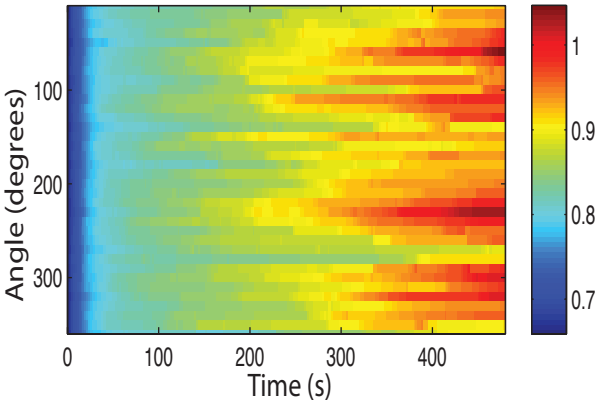

(ii) Velocity Map

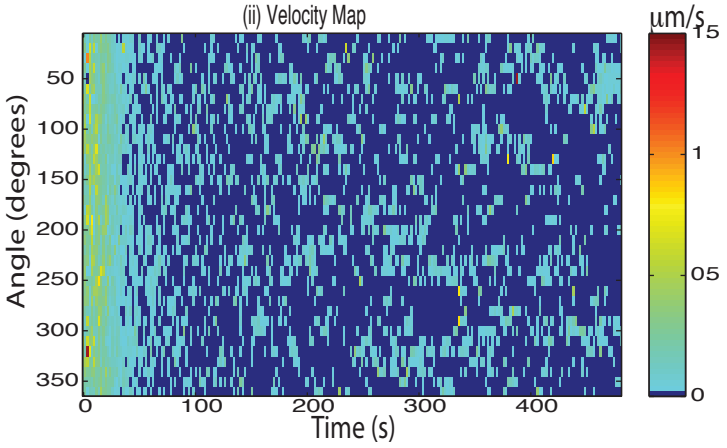

(iii) Fold change in radius

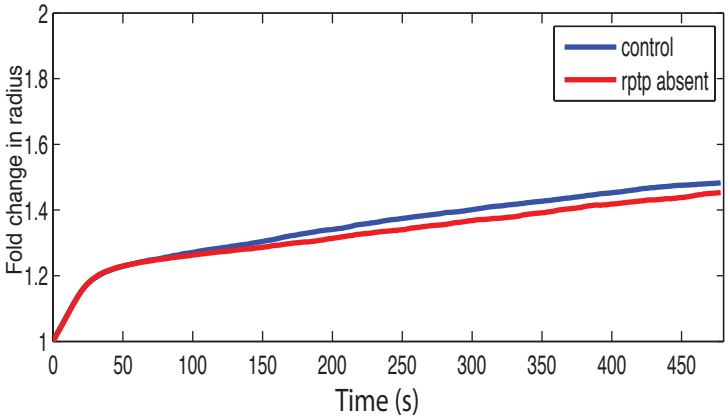

(iv) Circularity

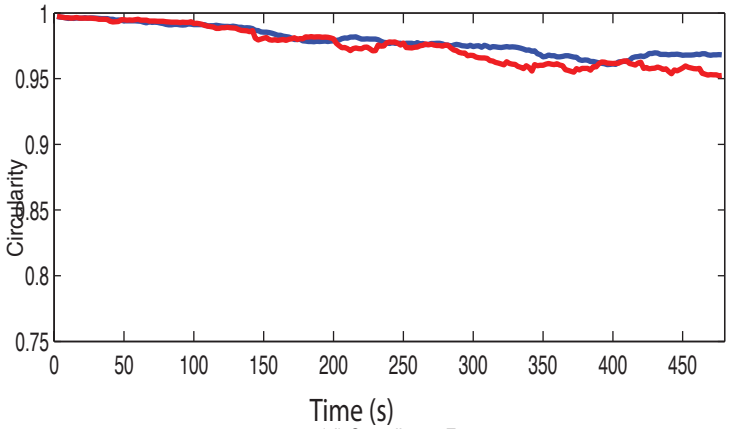

(v) Observed Rate of Polymerization

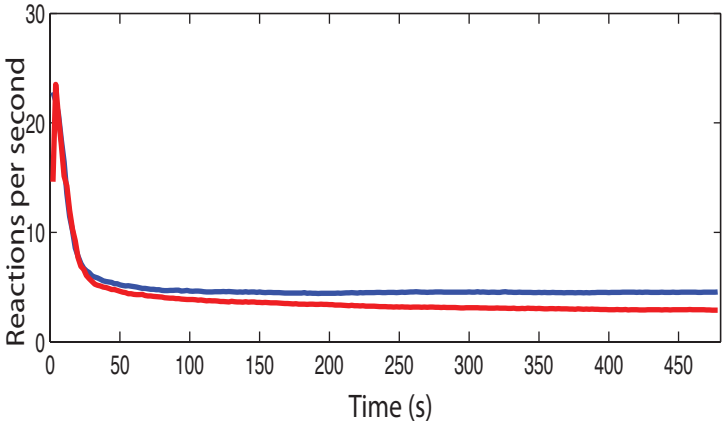

(vi) Compliance Factor

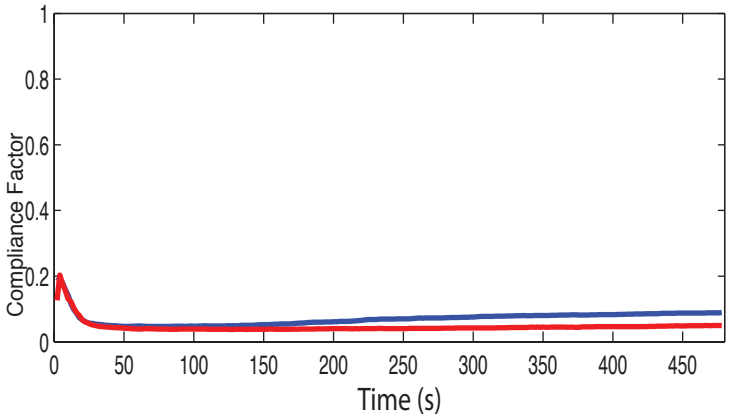

Figure S13

(A) Concentration Profiles

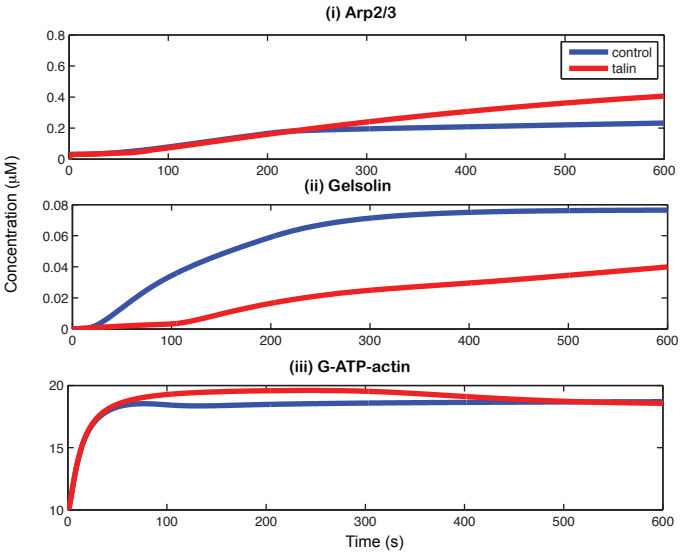

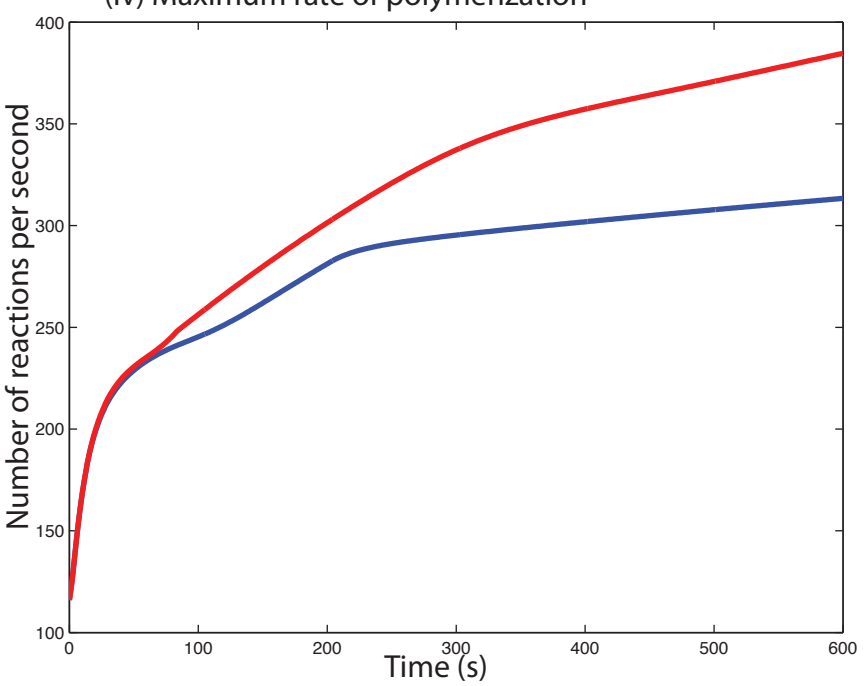

(B) Spreading Behavior

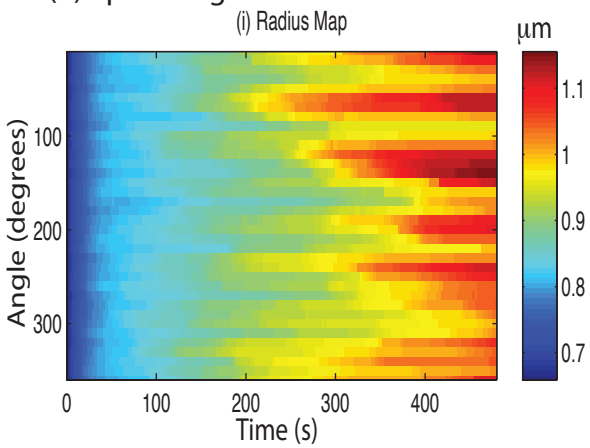

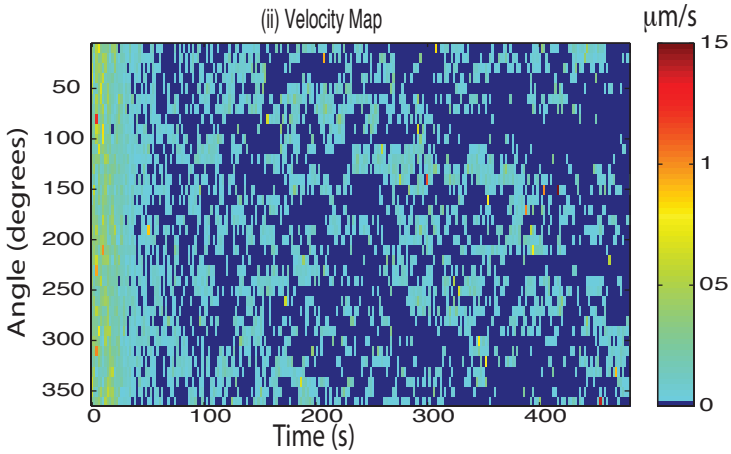

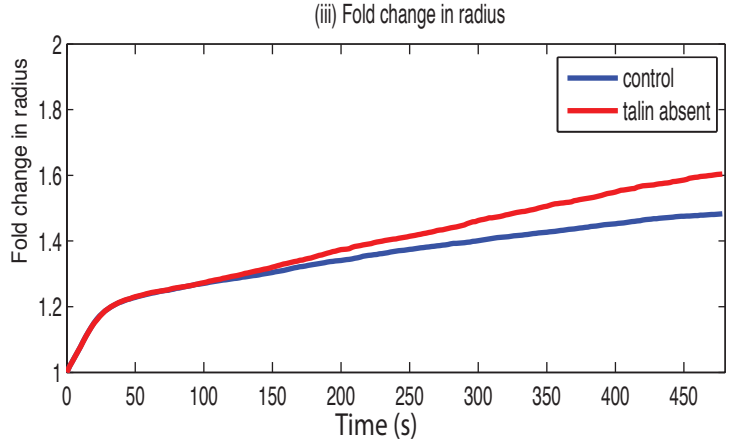

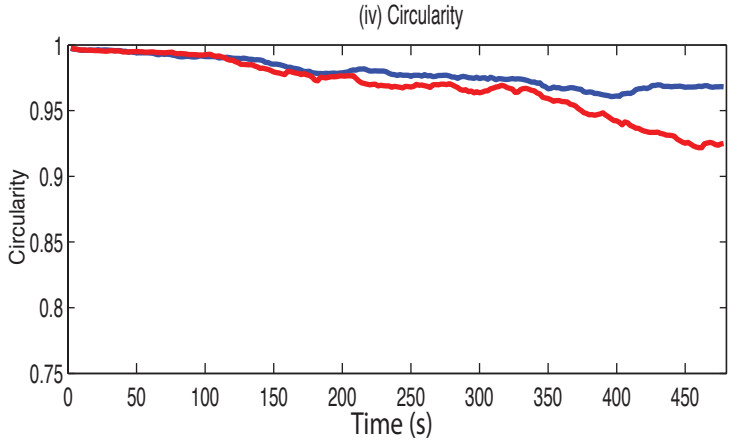

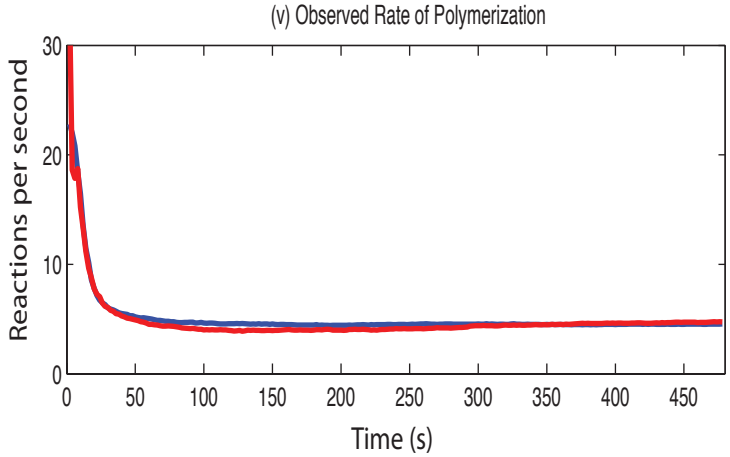

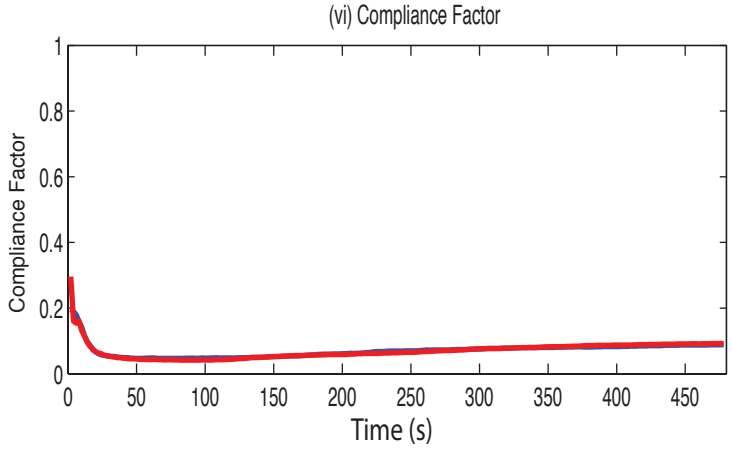

Figure S14

(A) Concentration Profiles

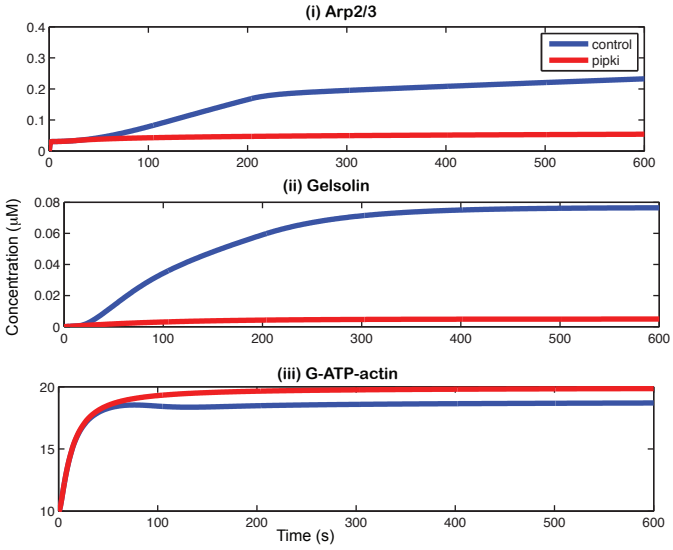

(iv) Maximum rate of polymerization

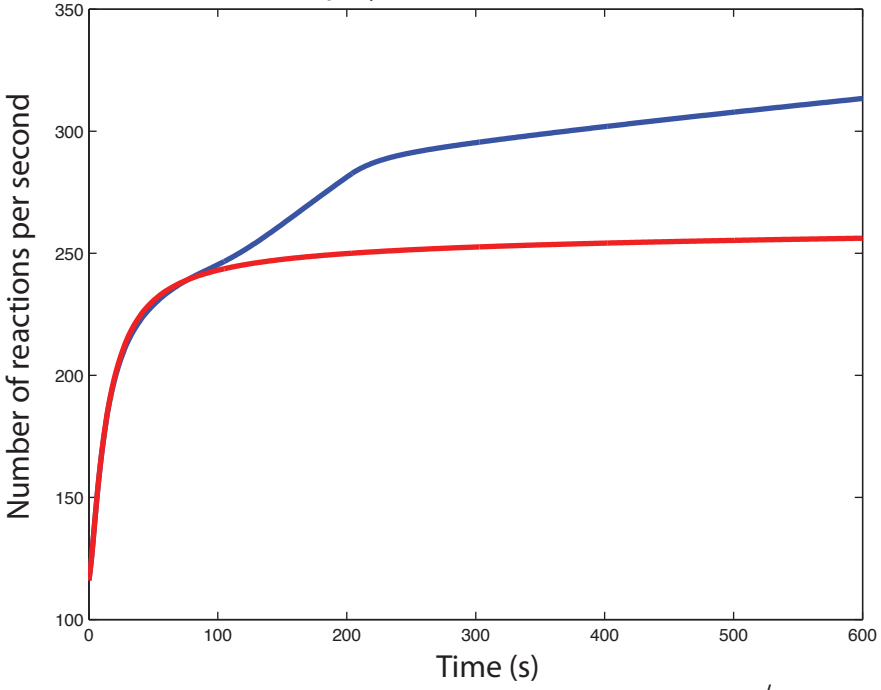

(B) Spreading behavior

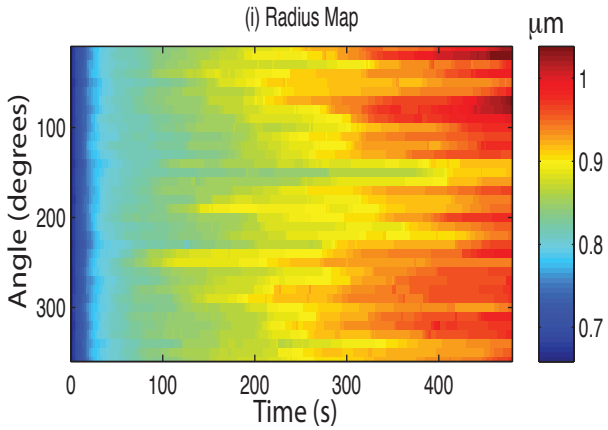

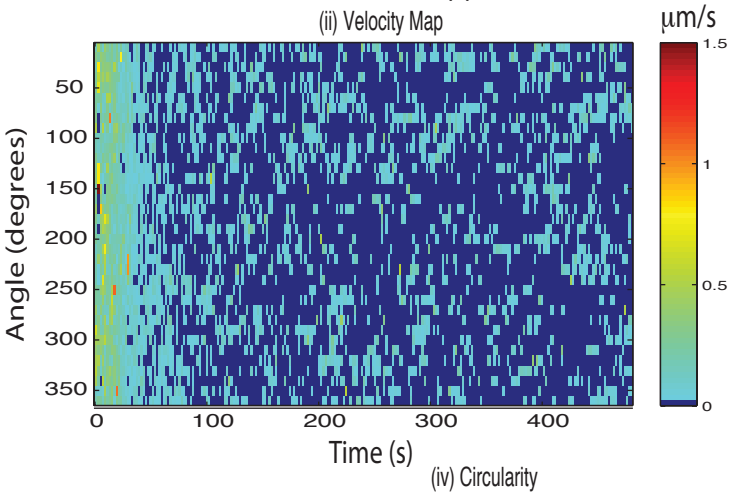

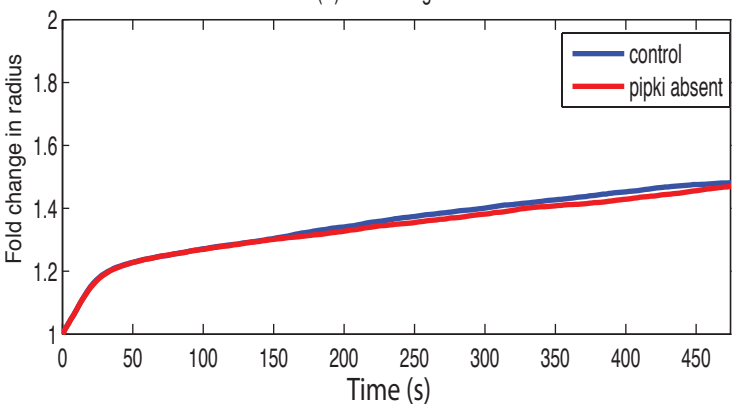

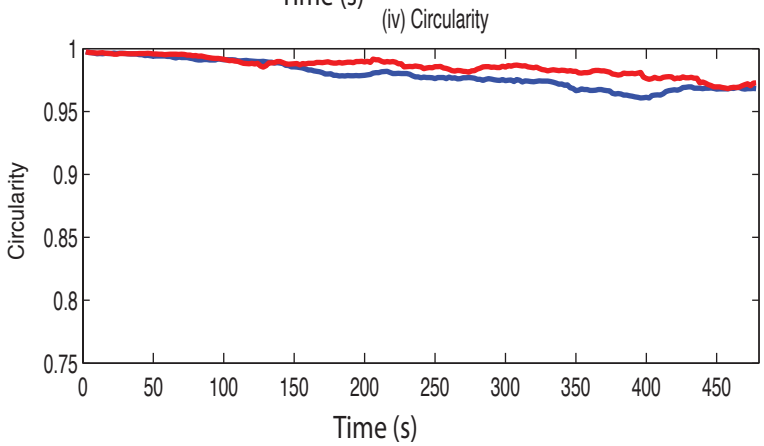

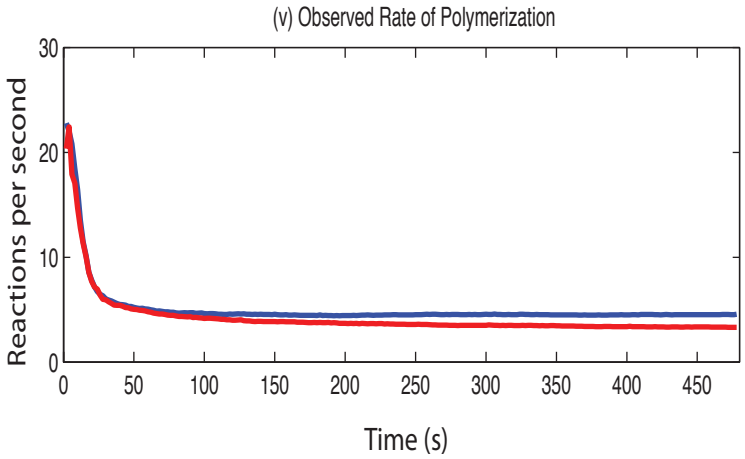

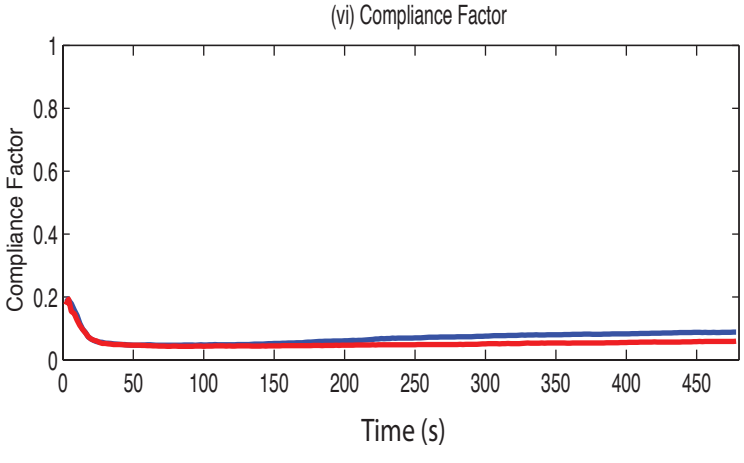

Figure S15

(A) Concentration Profiles

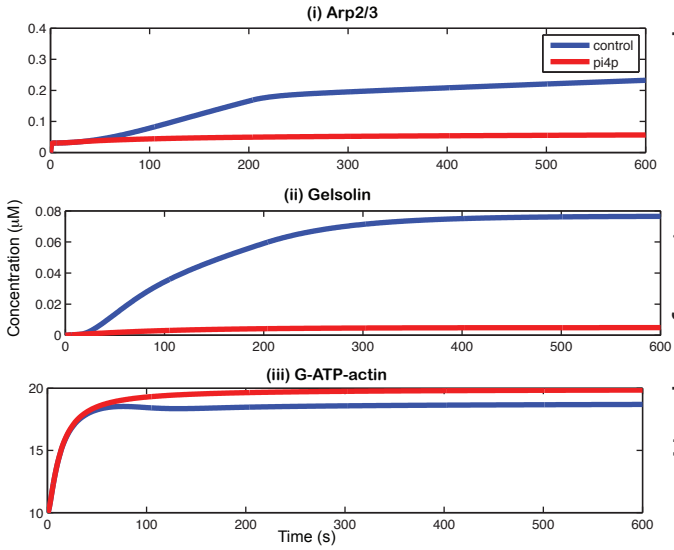

(iv) Maximum rate of polymerization

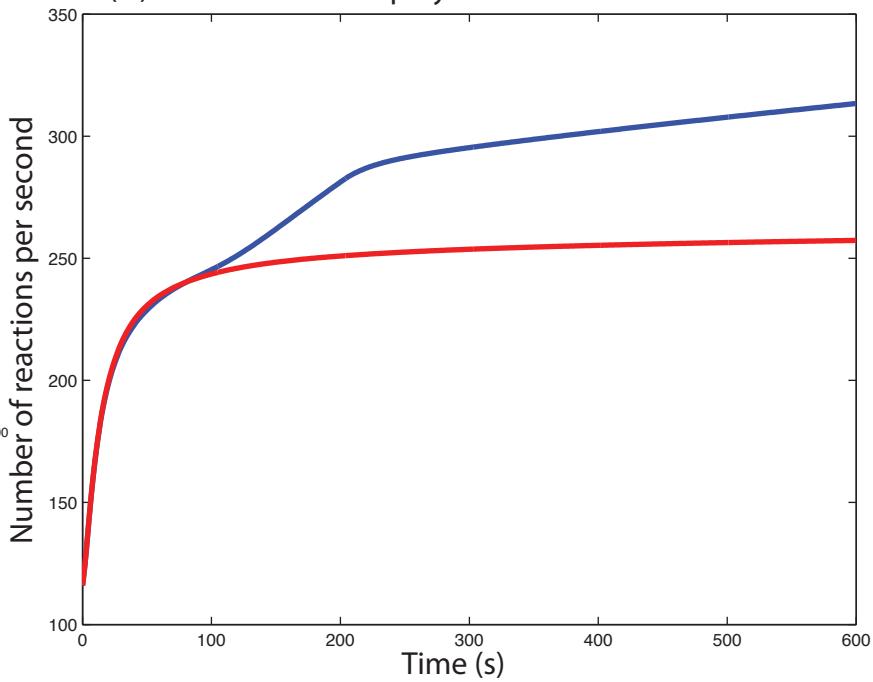

(B) Spreading Behavior

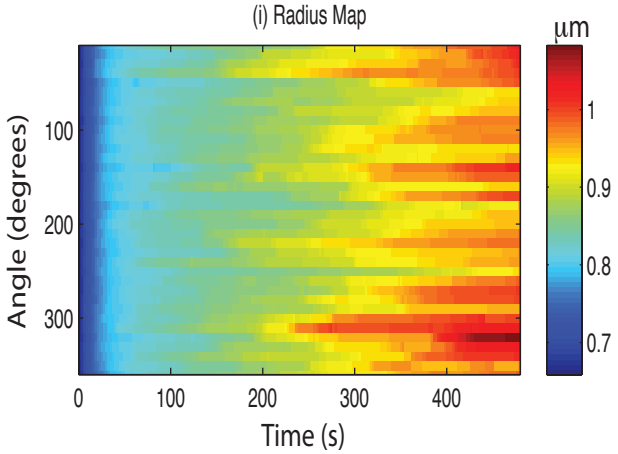

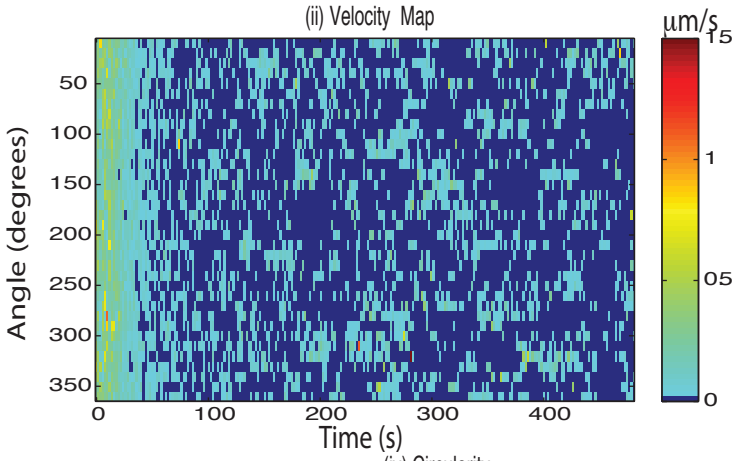

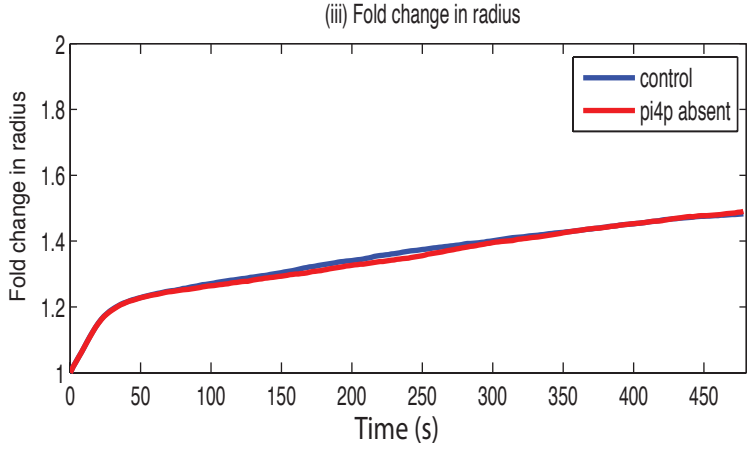

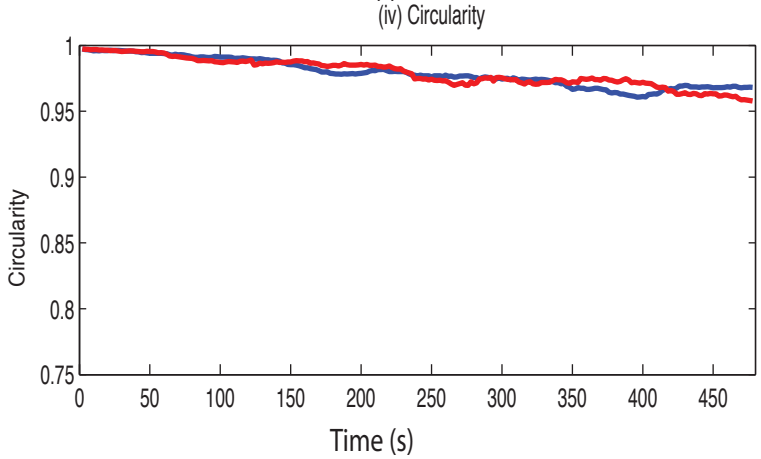

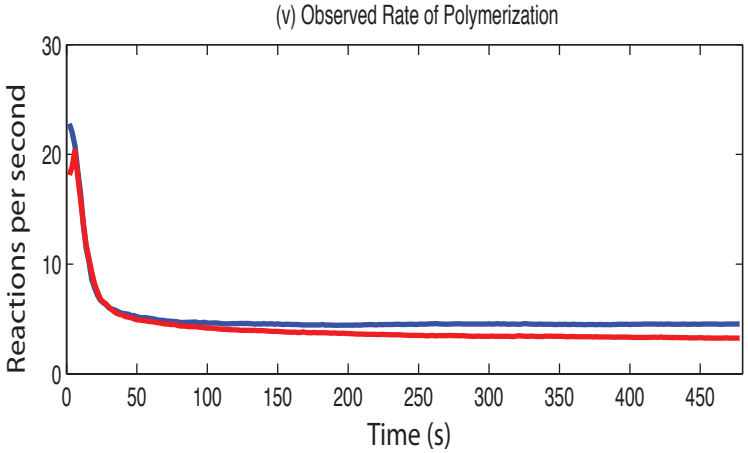

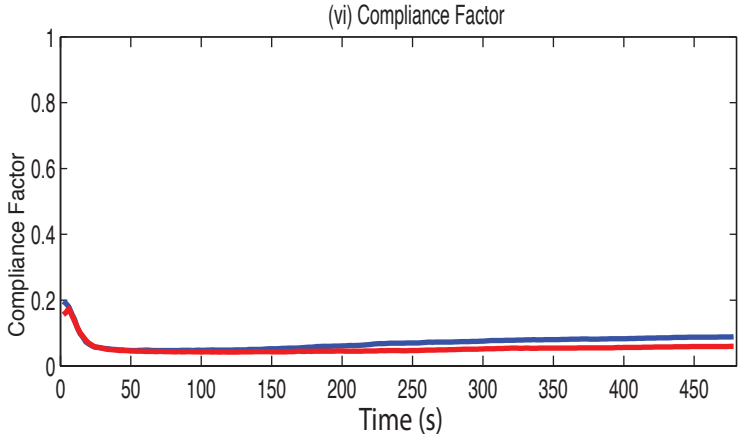

Figure S16

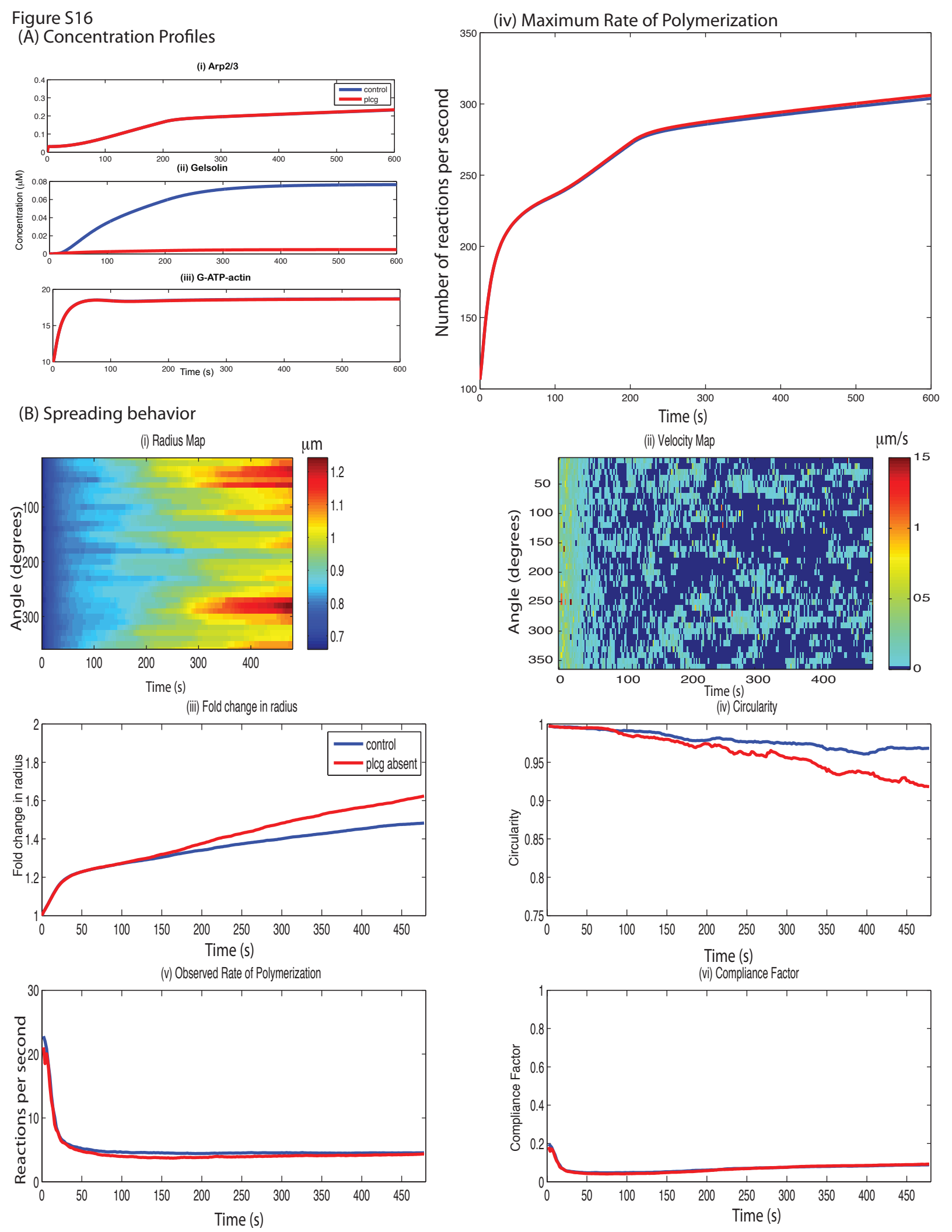
(A) Concentration Profiles
(i) Arp2/3
control
plcg
(ii) Gelsolin
Concentration (μM)
(iii) G-ATP-actin
Time (s)
(iv) Maximum Rate of Polymerization
Number of reactions per second
Time (s)
(B) Spreading behavior
(i) Radius Map
μm
Angle (degrees)
Time (s)
(ii) Velocity Map
μm/s
Angle (degrees)
Time (s)
(iii) Fold change in radius
control
plcg absent
Fold change in radius
Time (s)
(iv) Circularity
Circularity
Time (s)
(v) Observed Rate of Polymerization
Reactions per second
Time (s)
(vi) Compliance Factor
Compliance Factor
Time (s)

Figure S17

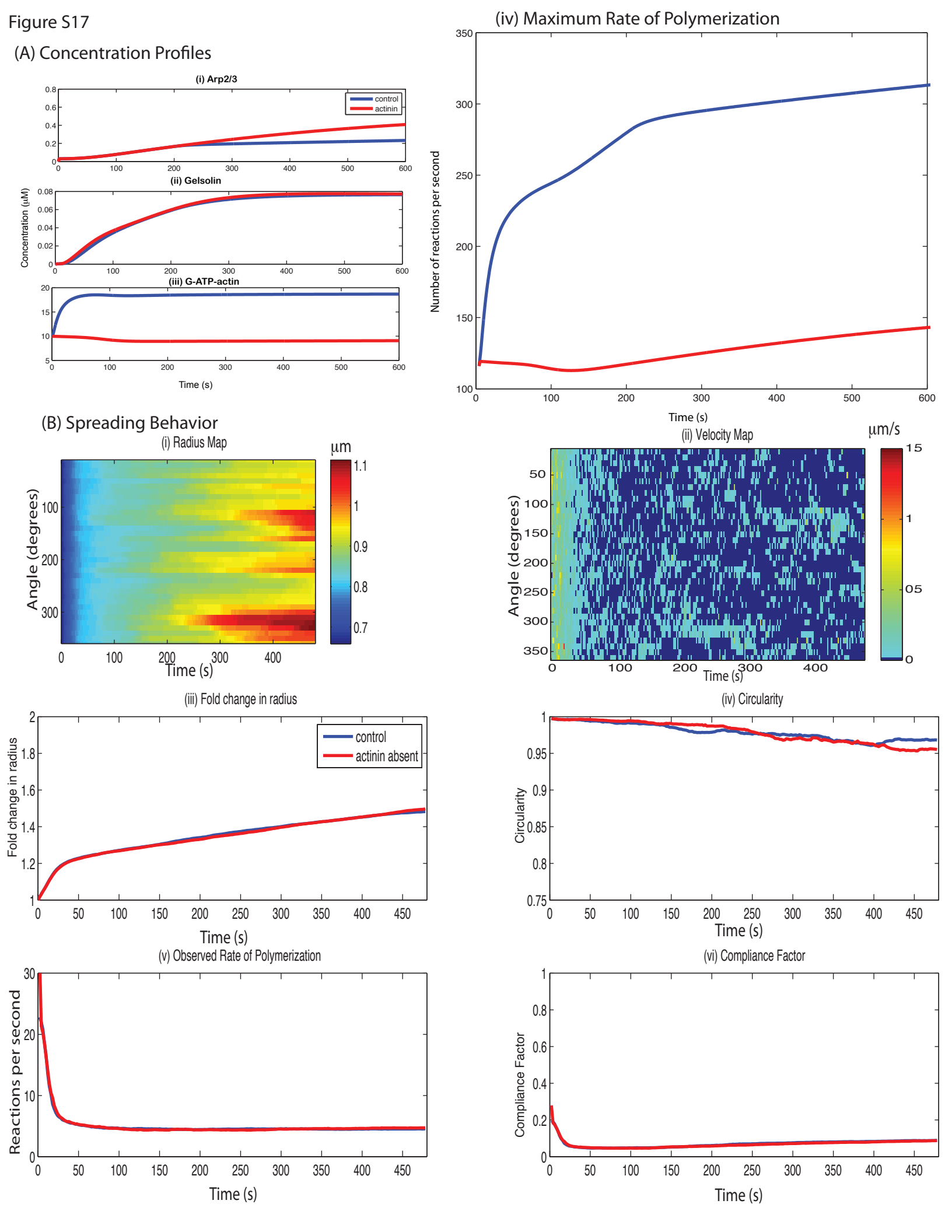
(A) Concentration Profiles
(i) Arp2/3
control
actinin
(ii) Gelsolin
Concentration (μM)
(iii) G-ATP-actin
Time (s)
(iv) Maximum Rate of Polymerization
Number of reactions per second
Time (s)
(B) Spreading Behavior
(i) Radius Map
μm
Angle (degrees)
Time (s)
(ii) Velocity Map
μm/s
Angle (degrees)
Time (s)
(iii) Fold change in radius
control
actinin absent
Fold change in radius
Time (s)
(iv) Circularity
Circularity
Time (s)
(v) Observed Rate of Polymerization
Reactions per second
Time (s)
(vi) Compliance Factor
Compliance Factor
Time (s)

Figure S18

(A) Kb=0

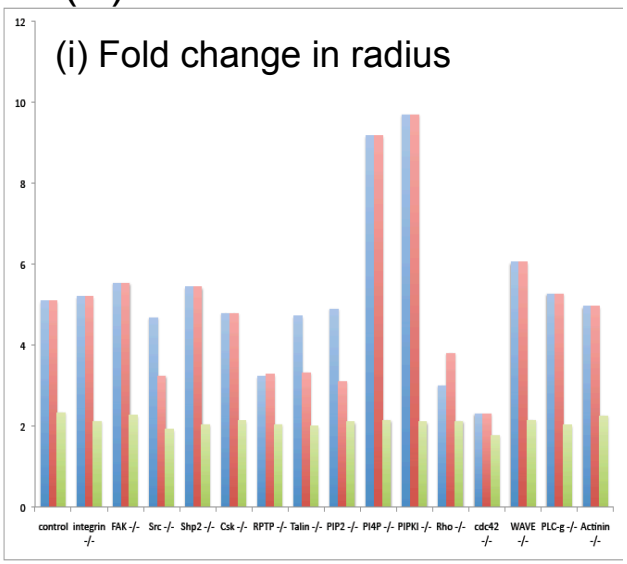

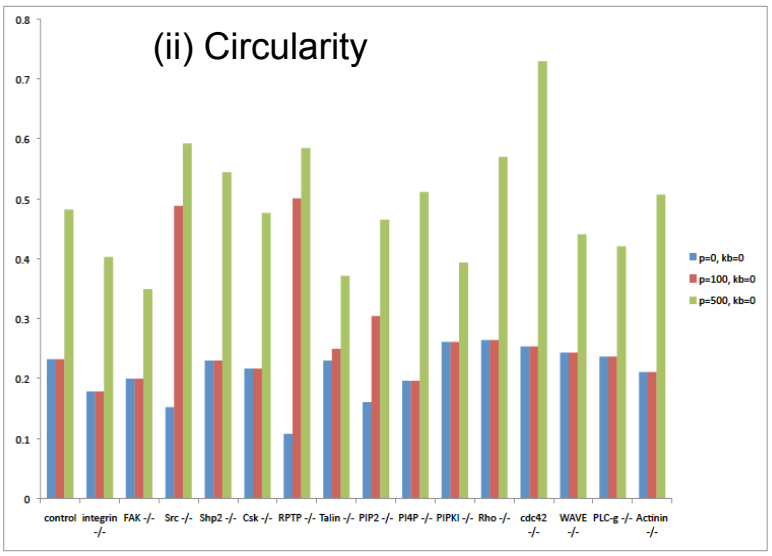

(B) Kb=0.08

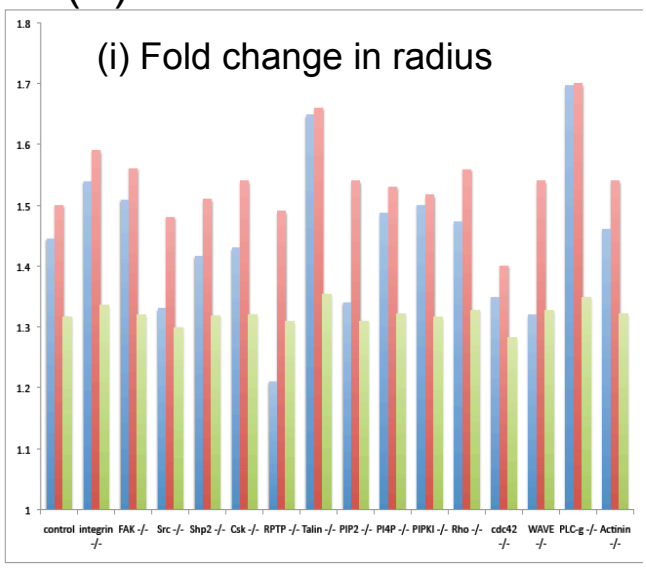

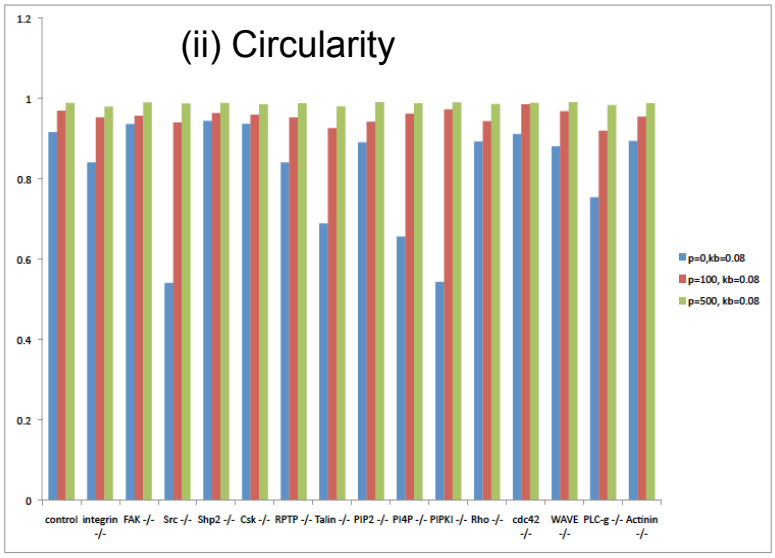

(C) Kb=0.2